Thermochemistry and Reactivity of Cationic Scandium and Titanium Sulfide in the Gas Phase

Ilona Kretzschmar, Detlef Schröder, and Helmut Schwarz*

Institut für Organische Chemie der Technischen Universität Berlin, Strasse des 17. Juni 135, D-10623 Berlin, Germany

Chad Rue and P. B. Armentrout*

Department of Chemistry, University of Utah, Salt Lake City, Utah 84112

Received: November 30, 1999; In Final Form: March 7, 2000

The gas-phase reactivities of the transition-metal sulfides ScS^+ and TiS^+ are investigated with guided-ion beam (GIB) and Fourier transform ion cyclotron resonance (FTICR) mass spectrometry. In this work, we study the reactions of bare Sc^+ and Ti^+ ions with sulfur-transfer reagents, COS and CS_2, and of the metal sulfides, ScS^+ and TiS^+, with oxygen-transfer substrates and with Xe to examine their collision-induced dissociation. The GIB experiments lead to several estimates for $D_0(M^+-S)$. Further, the reaction $MS^+ + H_2O \rightarrow MO^+ + H_2S$ and its reverse are studied with GIB and FTICR. The equilibrium constants K_{eq} derived from these measurements provide the most accurate values for $D_0(M^+-S)$. Overall assessment of the results of ion−molecule reactions, collision-induced dissociations, and equilibrium measurements yields the 0 K bond dissociation energies $D_0(Sc^+-S) = 4.97 \pm 0.05$ eV, $D_0(Ti^+-S) = 4.74 \pm 0.07$ eV, $D_0(Sc^+-CS) = 1.38 \pm 0.08$ eV, $D_0(Ti^+-CS) = 1.60 \pm 0.06$ eV, and $\Delta_f H_0(TiOS^+) = 9.04 \pm 0.18$ eV.

Introduction

Interest in transition-metal sulfides arises from their significance in industrial catalysis and biology.[1] Although, no biological relevance has yet been attributed to scandium and titanium sulfides, these materials play a role in other areas of research, ranging from astrophysics to material sciences and the steel industry. Titanium sulfides, for example, are used as additives for extra-low-carbon steels to enhance the fishscale resistance (H_2 permeablility) and the adherence of steel.[2] Further, spectral lines observed in the near-infrared region of molecular spectra of S-type stars have been assigned to the electronic transitions of the TiS molecule.[3] The knowledge of accurate bond-dissociation energies together with reported values for $D_0(M-S)$[4,5] will allow the estimation of ionization energies (IEs), which in turn enable spectroscopists to use more accurate methods for the determination of IE(MS) with uncertainties below 5 meV, such as two-color photoionization (R2PI) spectroscopy.[6] Another application of accurate experimental bond-dissociation energies is their use as benchmarks for quantum chemistry. In analogy to the metal-oxide cations,[7] the valence space of the electronic ground state of ScS^+ should be represented by a $1\sigma^2 2\sigma^2 1\pi^4$ configuration. This configuration suggests that ScS^+ is a closed-shell singlet with only bonding orbitals occupied.[8] Addition of electrons as one moves to the right in the periodic table requires occupation of nonbonding or antibonding orbitals. Thus, ScS^+ and TiS^+ are suitable molecules for testing the performance of high-level ab initio methods in the description of transition-metal sulfides, and the knowledge of accurate bond-dissociation energies will aid this task.

As part of an ongoing series of investigations,[9−11] this article is designed to establish an accurate database for bond-dissociation energies (D_0) of cationic scandium and titanium sulfides and thiocarbonyls. Previous work on the analogous vanadium systems[10] has shown that accurate thermochemistry can be established using two distinct mass spectrometric methods, that is, guided-ion beam mass spectrometry and Fourier transform ion cyclotron mass spectrometry. These methods are used to study the reactions of atomic Sc^+ and Ti^+ with COS and CS_2 and the reactions of ScS^+ and TiS^+ with oxygen-transfer reagents and Xe. Additionally, reaction rate constants are derived for the $MS^+ + H_2O \rightleftarrows MO^+ + H_2S$ equilibrium. This experimental work is then augmented with theoretical calculations designed to establish the appropriate electronic states to consider.

Experimental and Computational Methods

Two entirely different, but complementary mass-spectrometric methods are applied in this study. The guided-ion beam (GIB) technique is used for the evaluation of thermodynamic data by means of threshold measurements of endothermic reactions, whereas Fourier transform ion cyclotron resonance (FTICR) mass spectrometry allows the assessment of rate coefficients for exothermic processes. Provided that neither activation barriers nor Gibbs free energies are too large, equilibrium constants can also be determined using FTICR.

Guided-Ion Beam. Detailed descriptions of the GIB apparatus used in this study and the experimental procedures are given elsewhere.[12,13] Ar^+ ions created in a dc discharge source[13] are accelerated toward a metal cathode thereby sputtering off M^+ ions (M = Sc, Ti). The metal ions drift in a meter-long flow tube operated with a 9:1 mixture of helium and argon at pressures of ~0.7 Torr. The ions undergo $\sim 10^5$ collisions with the buffer gas before exiting the flow tube and therefore are expected to equilibrate to room temperature.[14] In addition, methane is introduced ca. 25 cm downstream from the discharge at pressures between 0.5 and 4 mTorr, because helium and argon

10.1021/jp994228o CCC: $19.00
Published on Web 05/04/2000

do not always effectively quench excited states of atomic transition-metal ions.[15] Operation at these pressures allows the ions to undergo 10^2-10^3 collisions with methane in the flow tube before they react with the neutral reagents of interest in the GIB device. This is sufficient to remove virtually all excited states of the metal ions under study.[16]

After extraction from the source, the ions are accelerated and focused into a magnetic sector, mass-selected, decelerated to a desired kinetic energy, and focused into an octopole ion trap.[12] This device guides the ions through a static gas cell kept at a low pressure ($\sim$ 0.05−0.1 mTorr) of the reactant gas. It is verified that all product cross-sections reported correspond to single ion−molecule collisions by examining the pressure dependence of the product intensities. After exiting the gas cell, product and unreacted beam ions drift to the end of the octopole where they are directed into a quadrupole mass filter for mass analysis and then detected. Conversion of the raw ion intensities into reaction cross-sections and the calibration of the absolute energy scale are treated as described previously.[12] The accuracy of the absolute cross-sections is estimated to be ±20%. The beams have Gaussian kinetic energy distributions with average full widths at half-maximum (fwhm) of ca. 0.25 eV in the laboratory frame. The uncertainty of the absolute energy scale is ±0.05 eV (lab).

Quantitative analysis of the energy dependence of these cross-sections is achieved using eq 1 and methods outlined elsewhere.[17]

$$\sigma(E) = \sigma_0 \Sigma g_i (E + E_i - E_0)^n / E \qquad (1)$$

In eq 1, E is the relative kinetic energy of the reactants, E_0 is the threshold for reaction at 0 K, σ_0 is a scaling parameter, and n is a fitting parameter. The summation is over the rovibrational states of the reactants having energies E_i and populations g_i ($\Sigma g_i = 1$). Before comparison with the data, this equation is convoluted over the translational energy distributions of both reactants. This determination of the reaction thresholds involves explicit consideration of the distributions of vibrational, rotational, and translational energies of both reactants. Because all sources of reactant energy are considered, the thermochemistry obtained corresponds to 0 K values in all cases.

The MX^+ ions (X = O, S) are generated by addition of O_2 and COS, respectively, to the flow 75 cm downstream from the source. For TiS^+, a problem of mass overlap with the isobaric Ar_2^+ dimer ($m/z = 80$) is encountered. To minimize interferences, p_{COS} and p_{Ar} are varied until an optimum ratio of TiS^+/Ar_2^+ is reached. The amount of Ar_2^+ in the TiS^+ beam is probed by collisional-induced dissociation (CID) with xenon, yielding Ar^+ and Xe^+ as characteristic products that have cross-sections smaller than 0.20 and 0.35×10^{-16} cm^2, respectively, if the partial pressures of Ar and COS are adjusted optimally. According to these measurements, the fraction of Ar_2^+ left in the TiS^+ beam amounts to 2−5%. The contributions from reactions of the neutral targets with Ar_2^+ to the product cross-sections of the TiS^+/neutral systems are monitored by examination of all reactions with pure Ar_2^+ beams. For the Ar_2^+/CO system, signals are observed at $m/z = 28$, 40, and 44; for the Ar_2^+/CO_2, system, they are observed at 40 and 44; and for the Ar_2^+/COS system, products are observed at $m/z = 28$, 32, 40, 44, 60, and 64.[17] Comparison of the cross-sections obtained for the Ar_2^+/X measurements with those of the TiS^+/X systems ($m/z = 48$, 60, and 64 for X = CO; $m/z = 48$, 64, and 96 for X = CO_2; $m/z = 48$, 64, and 112 for X = COS) reveals that only the TiS^+/COS and Ar_2^+/COS systems share a common product, $m/z = 64$. Using the cross-section at $m/z = 32$ ($\sigma_{max,32} = 0.14 \times 10^{-16}$ cm^2) of the TiS^+/COS system, which results from the Ar_2^+ impurity in the putative TiS^+ and is the main product of the pure Ar_2^+/COS system ($\sigma_{max,32} = 6.94 \times 10^{-16}$ cm^2 and $\sigma_{max,64} = 0.6 \times 10^{-16}$ cm^2), it becomes clear that the contribution to $m/z = 64$ ($\sigma_{max,64} = 0.85 \times 10^{-16}$ cm^2) in the TiS^+/COS system from the reaction of Ar_2^+ with COS is $\sigma_{max,64} = 0.01 \times 10^{-16}$ cm^2, and thus negligible.

Fourier Transform Ion Cyclotron Resonance. A Spectrospin CMS-47X FTICR mass spectrometer with an external ion source[19] is used to investigate the exothermic formations of MS^+ in the reactions of the transition-metal cations M^+ and their oxides MO^+ with CS_2, COS, and H_2S, as well as the formation of MO^+ in the reaction of MS^+ with H_2O. The M^+ ions are generated via laser desorption/laser ionization by focusing the beam of a Nd:YAG laser (Spectron Systems, $\lambda = 1064$ nm) onto a metal target. The ions are extracted from the source and transferred into the analyzer cell by a system of electrostatic potentials and lenses. After deceleration, the ions are trapped in the field of a superconducting magnet (maximum field strength, 7.05 T). The most abundant isotope (^{45}Sc and ^{48}Ti, respectively) is mass-selected using FERETS,[20] a computer-assisted protocol that combines frequency sweeps and single-frequency ion-ejection pulses to optimize ion isolation. Generation of the MO^+ and MS^+ ions is achieved by reaction of M^+ with pulsed-in O_2 and COS, respectively. For the purpose of thermalization, the ions are collided with pulsed-in methane (maximum pressure ca. 3×10^{-5} Torr, ca. 2000 collisions) before reaction. The kinetic values of all reactions are studied carefully as a function of thermalizing collisions to ensure that the ions undergoing subsequent ion−molecule reactions are not kinetically and/or electronically excited. The reactants are admitted to the cell via leak valves at stationary pressures between 1 and 10×10^{-8} Torr (as measured by a Balzers IMG070 ion gauge). The first-order kinetics of the reacting ions provides the rate constants, k_{exp}, which are compared with the gas-kinetic collision rates,[21] k_c, in terms of reaction efficiencies $\phi = k_{exp}/k_c$.

Calculations. The bond lengths and the ground-state/excited-state splittings of MS^+ (M = Sc, Ti) are calculated with density functional theory (DFT). The DFT calculations are performed using the Amsterdam density functional (ADF, version 2.0.1) suite of programs[22] with the inner-shell electrons ([Ne] for S and [Ar] for M) treated in the frozen-core approximation.[23] The valence orbitals are expanded as linear combinations of Slater-type basis functions. Triple-ζ basis sets are used for scandium, titanium, and sulfur. All molecular and atomic energies are calculated using the local spin-density approximation (LDA) with Slater's exchange functional and the Vosko−Wilk−Nusair parametrization (VWN)[24] augmented by Becke[25] and Perdew's[26] (BP) gradient corrections for the exchange and correlation potentials, respectively.[27] This method will be referred to as ADF/BP. The ADF program has advantages because it provides control over the symmetry of the wave function created during geometry optimizations and it permits the calculations of the excited states.

Results

In this section, we report the gas-phase reactivity of ScS^+ and TiS^+ obtained with two complementary mass-spectrometric techniques. First, the formation of MS^+ (M = Sc, Ti) is studied by reacting the bare transition-metal cations with the sulfur-transfer reagents COS and CS_2. Next, the CID of MS^+ ions is

TABLE 1: Heats of Formation and Bond-Dissociation Energies for Ionic Species at 0 K

ionic species	$\Delta_f H°$ (eV)[a]	bond	D_0 (eV)
Sc^+	10.46 (0.08)[b]		
Ti^+	11.70 (0.07)[c]		
ScC^+	14.49 (0.10)	Sc^+-C	3.34 ± 0.06[d]
TiC^+	15.02 (0.25)	Ti^+-C	4.05 ± 0.24[d]
ScO^+	5.88 (0.10)	Sc^+-O	7.14 ± 0.06[d]
TiO^+	7.38 (0.10)	Ti^+-O	6.88 ± 0.07[d]
ScS^+	8.32 (0.09)	Sc^+-S	4.97 ± 0.05*
TiS^+	9.81 (0.10)	Ti^+-S	4.74 ± 0.07*
$ScCO^+$	8.62	Sc^+-CO	0.66[e]
$TiCO^+$	9.30 (0.09)	Ti^+-CO	1.22 ± 0.06[f]
$ScCS^+$	11.93 (0.12)	Sc^+-CS	1.38 ± 0.08*
$TiCS^+$	12.95 (0.10)	Ti^+-CS	1.60 ± 0.06*
ScO_2^+	6.72 (0.21)	OSc^+-O	1.72 ± 0.19[g]
TiO_2^+	6.44 (0.14)	OTi^+-O	3.50 ± 0.10[h]
$TiOS^+$	9.04 (0.18)	STi^+-O	3.33 ± 0.15*
		OTi^+-S	1.19 ± 0.20*

[a] If not stated otherwise, these values are calculated from the data given in Tables 1 and 2. [b] Wagman, D. D.; Evans, W. H.; Parker, V. B.; Schumm, R. H.; Halow, I.; Bailey, S. M.; Churney, K. L., Nuttall, R. L. *J. Phys. Chem. Ref. Data* **1982**, *11* (Suppl 2). [c] Chase, M. W., Jr.; Davies, C. A.; Downey, J. R., Jr.; Frurip, D. J.; McDonald, R. A.; Syverud, A. N. *J. Phys. Chem. Ref. Data* **1985**, *14* (Suppl. 1) (JANAF Tables). [d] Clemmer, D. E.; Elkind, J. L.; Aristov, N.; Armentrout, P. B. *J. Chem. Phys.* **1991**, *95*, 3387. [e] Theoretical estimate taken from ref 33. [f] Ref 34. [g] Ref 35. [h] Ref 36. *This work.

probed by colliding MS^+ ions with xenon in the GIB instrument. Further, the reactivity of MS^+ ions (M = Sc, Ti) toward the oxygen compounds CO, CO_2, and COS is investigated so that the formation of thermodynamically well-characterized species, such as M^+ and MO^+ (M = Sc, Ti), can be used as means for the refinement of $D_0(M^+-S)$. Finally, reaction 2 and its reverse (2′) are measured with GIB and FTICR.

$$MS^+ + H_2O \rightleftarrows MO^+ + H_2S \qquad (2)$$

As an independent determination of $D_0(M^+-S)$, the equilibrium constants K_{eq} are derived as the quotient of the rate constants determined with GIB and FTICR for reactions 2 and 2′. Subsequently, $K_{eq}(2)$ is converted into $\Delta_R G_{298}(2)$ by means of the Gibbs−Helmholtz equation and then converted to $\Delta_R H_0(2)$ to independently derive $D_0(M^+-S)$.[11g,28,29] The thermochemical data used in this study are summarized in Tables 1 and 2. The section is completed by a brief description of the theoretical results.

Reactions of M^+ with COS. The cross-sections measured for the reactions of M^+ (M = Sc, Ti) with carbonyl sulfide under GIB conditions are shown in Figure 1. Three processes are observed and can be assigned to formation of MS^+, MO^+, and MCO^+ in reactions 3−5, respectively.

$$M^+ + COS \rightarrow MS^+ + CO \qquad (3)$$

$$\rightarrow MO^+ + CS \qquad (4)$$

$$\rightarrow MCO^+ + S \qquad (5)$$

The results are similar for both metals, except that reaction 5 is somewhat less efficient for scandium. The exothermic formation of MS^+ (M = Sc, Ti) according to reaction 3 dominates the whole energy range studied (Tables 3 and 4).

In general, cross-sections for exothermic ion−molecule reactions decline with an energy dependence proportional to $E^{-1/2}$, as predicted by the Langevin−Gioumousis−Stevenson (LGS) model[30] for collisions between ions and molecules at elevated kinetic energies, eq 6.

TABLE 2: Heats of Formation and Bond-Dissociation Energies for Neutral Species at 0 K[a]

neutral species	$\Delta_f H°$ (eV)	bond	D_0 (eV)
C	7.371 (0.005)		
S	2.847 (0.003)		
D	2.278	D−D	4.556
O	2.558 (0.001)	O−O	5.116 (0.001)
CO	−1.180 (0.002)	C−O	11.109 (0.005)
OD	0.382 (0.003)[b]	O−D	4.454 (0.003)
SD	1.43 (0.05)	S−D	3.70 (0.05)
CS	2.85 (0.04)[c]	C−S	7.37 (0.04)
SO	0.052 (0.013)	S−O	5.353 (0.013)
S_2	1.330 (0.003)	S−S	4.364 (0.005)
CS_2	1.200 (0.008)[d]	SC−S	4.50 (0.04)
COS	−1.473 (0.003)[d]	OC−S	3.140 (0.005)
		SC−O	6.88 (0.04)
CO_2	−4.075 (0.001)	OC−O	5.453 (0.002)
SO_2	−3.075 (0.004)	OS−O	5.974 (0.014)
		$S-O_2$	5.922 (0.005)
H_2O	−2.476 (0.001)	H_2-O	5.034 (0.001)
D_2O	−2.552 (0.001)[b]	D_2-O	5.110 (0.001)
		DO−D	5.212 (0.003)
H_2S	−0.182 (0.008)	H_2-S	3.029 (0.009)
D_2S	−0.218 (0.008)	D_2-S	3.065 (0.009)
		DS−D	3.93 (0.05)

[a] Unless noted otherwise taken from: Chase, M. W., Jr.; Davies, C. A.; Downey, J. R., Jr.; Frurip, D. J.; McDonald, R. A.; Syverud, A. N. *J. Phys. Chem. Ref. Data* **1985**, *14* (Suppl. 1) (JANAF Tables). [b] Gurvich, L. V.; Veyts, I. V.; Alcock, C. B. *Thermodynamic Properties of Individual Substances*, 4th ed.; Hemisphere: New York, 1989; Vol. 1, Part 2. [c] Prinslow, D. A.; Armentrout, P. B. *J. Chem. Phys.* **1991**, *94*, 3563. [d] Pedley, J. B.; Naylor, R. D.; Kirby, S. P. *Thermochemical Data of Organic Compounds*; Chapman and Hall: London, 1986. Corrected to 0 K using values by, Wagman, D. D.; Evans, W. H.; Parker, V. B.; Schumm, R. H.; Halow, I.; Bailey, S. M.; Churney, K. L., Nuttall, R. L. *J. Phys. Chem. Ref. Data* **1982**, *11* (Suppl. 2).

$$\sigma_{LGS} = \pi e(2\alpha/E)^{1/2} \qquad (6)$$

Here, α is the polarizability of COS (5.71 Å^3),[31] and E is the relative kinetic energy of the reactants. If the molecule is polar, then an upper limit to the cross-section is given by the locked-dipole (LD) formula, eq 7,[32] where μ_D is the permanent dipole moment of the neutral reactant.

$$\sigma_{LD} = \sigma_{LGS} + \pi e\mu_D/E \qquad (7)$$

Both MS^+ cross-sections deviate from σ_{LGS} (solid lines, Figure 1). Fitting of the ScS^+ and TiS^+ cross-sections at energies below about 1.0 eV (dashed lines in Figure 1) yields exponential functions, E^{-p}, with $p = 0.65 \pm 0.05$ and 0.90 ± 0.10 for ScS^+ and TiS^+, respectively. The behavior of the ScS^+ cross-section is almost Langevin-like, but with a reduced magnitude (ca. 0.3 σ_{LGS}), whereas the cross-section for TiS^+ shows an approximate E^{-1} dependence. Note that a deviation from Langevin points to the operation of significant kinetic hindrance en route to product formation. For example, the E^{-1} decline of the low-energy VS^+ cross-section in the V^+/COS system has been attributed to the spin-forbidden formation of VS^+ in its $^3\Sigma^-$ ground state, whereas a second feature at elevated energies has been assigned to the spin-allowed formation of VS^+ in the $^5\Pi$ excited state.[10] By analogy, the ScS^+ and TiS^+ cross-sections flatten out at energies greater than 1.0 eV, which plausibly is attributed to the formation of excited electronic states of ScS^+ and TiS^+ cations. The cross-sections continue to decline between 3 and 4 eV, which can be attributed to dissociation of the MS^+ products, beginning at $D_0(S-CO) = 3.14$ eV (Table 2).

TABLE 3: Summary of Parameters in eq 1 Used for Fitting the Cross-sections and the Derived $D_0(Sc^+-S)$ in eV

reaction				E_0, (eV)[a]	σ_0	n	$D_0(Sc^+-S)$ (eV)
$COS + Sc^+$	→	$ScS^+ + CO$	(3)	<0	119 (24)[b]		>3.14 (0.01)
	→	$ScO^+ + CS$	(4)	<0	36 (7)[b]		
$CS_2 + Sc^+$	→	$ScS^+ + CS$	(9)	<0	318 (30)[b]		>4.50 (0.01)
	→	$ScCS^+ + S$	(10)	3.12 (0.07)	3.06 (0.35)	1.4 (0.1)	
$Xe + ScS^+$	→	$Sc^+ + S + Xe$	(12)	5.74 (0.26)	2.11 (0.70)	1.7 (0.2)	<5.74 (0.26)
$CO + ScS^+$	→	$Sc^+ + COS$	(13)	2.10 (0.80)	0.13 (0.13)	1.6 (0.5)	5.24 (0.80)
	→	$ScO^+ + CS$	(14)	3.70 (0.27)	0.68 (0.23)	1.2 (0.2)	7.10 (0.28)
	→	$Sc^+ + CO + S$	(15)	5.92 (0.18)	0.80 (0.20)	1.9 (0.1)	<5.92 (0.18)
$CO_2 + ScS^+$	→	$ScO^+ + COS$	(19)	0.77 (0.08)	0.37 (0.01)	2.0 (0.1)	5.60 (0.10)
	→	$Sc^+ + S + CO_2$	(22)	5.64 (0.37)	0.34 (0.18)	2.0 (0.2)	<5.64 (0.37)
$COS + ScS^+$	→	$ScS_2^+ + CO$[c]	(24)	0.90 (0.19)	0.85 (0.25)	1.8 (0.2)	
	→	$ScO^+ + CS_2$	(25)	1.22 (0.39)	0.06 (0.04)	2.2 (0.2)	5.98 (0.40)
	→	$Sc^+ + S_2 + CO$	(26)	4.17 (0.13)	1.03 (0.18)	1.8 (0.1)	5.39 (0.13)
$D_2O + ScS^+$	→	$ScO^+ + D_2S$	(2)		323 (13)[b]		4.93 (0.07)
$D_2S + ScO^+$	→	$ScS^+ + D_2O$	(2′)		0.20 (0.06)[b]		
				0.17 (0.03)	0.07 (0.01)	0.12 (0.07)	4.93 (0.07)

[a] The E_0 values are the average of several threshold fits with uncertainties of one standard deviation. [b] Maximum cross-sections at $E_{CM} \approx 0.03$ eV in units of 10^{-16} cm^2. [c] Fitting parameters for the endothermic feature after subtraction of exothermic part (see text).

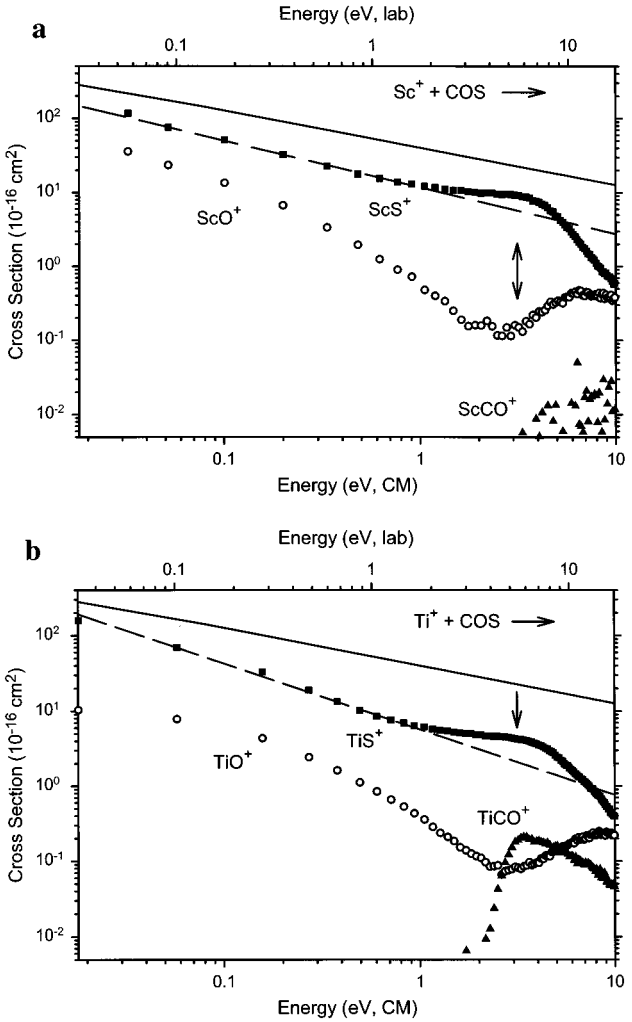

Figure 1. Product cross-sections for the reactions of M^+ (part a, M = Sc; part b, M = Ti) with COS to form MS^+ (■), MO^+ (○), and MCO^+ (▲) as functions of the center of mass energies (E_{CM}, lower axis) and laboratory energies (E_{lab}, upper axis). The arrow marks $D_0(S-CO) = 3.14$ eV. The solid lines represent σ_{LGS}, whereas the dashed lines show the fits of the exothermic features in the MS^+ cross-sections.

Less efficient low-energy processes observed in the M^+/COS systems lead to metal oxide cations according to reaction 4. Note that the cross-section for formation of TiO^+ is an order of magnitude smaller than $\sigma(TiS^+)$. Starting at 0.02 eV with cross-section magnitudes (Tables 3 and 4) of 36 and 10×10^{-16} cm^2, respectively, the MO^+ cross-sections decrease with increasing energy and thus are attributed to exothermic processes (Tables 3 and 4). This is consistent with the thermochemistry given in Tables 1 and 2, which results in $\Delta_R H_0 = -0.26 \pm 0.07$ eV and 0.00 ± 0.08 eV for reaction 4 with M = Sc and Ti, respectively. The cross-sections for the observed endothermic formation of MCO^+ in reaction 5 is very small for Sc^+ and not analyzed any further. The failure to observe efficient formation of $ScCO^+$ can be rationalized by the unfavorable thermochemistry of this channel, $D_0(Sc^+-CO) = 0.61$ eV[33] vs $D_0(S-CO) = 3.14 \pm 0.04$ eV, and competition with the exothermic reactions 3 and 4. The same reasons are believed to cause the threshold derived from the $TiCO^+$ cross-section, $E_0 = 2.57 \pm 0.07$ eV, to be somewhat above the thermochemical threshold of $\Delta_R H_0 = 1.92 \pm 0.06$ eV derived from $D_0(Ti^+-CO) = 1.22 \pm 0.06$ eV[34] and $D_0(S-CO) = 3.14 \pm 0.04$ eV. The decline of the $TiCO^+$ cross-section near 3 eV can be attributed to reaction 8, which starts at 3.14 eV.

$$Ti^+ + COS \rightarrow Ti^+ + CO + S \qquad (8)$$

The exothermicities of reactions 3 and 4 offer the opportunity to study them with FTICR mass spectrometry to determine rate coefficients and reaction efficiencies ϕ as defined above. Formation of MS^+ is observed upon trapping of bare M^+ ions (M = Sc, Ti) in COS in the FTICR, as expected for the exothermic behavior observed for processes 3 and 4 under GIB conditions. The observed reaction efficiencies $\phi(MS^+)$ for reaction 3 are 0.35 ± 0.07 and 0.37 ± 0.07 for M = Sc and Ti, respectively. The only other process observed in the FTICR experiments is formation of MO^+. However, in addition to the reagent of interest, background contaminants are present in the vacuum system, particularly O_2 and H_2O. Reactions of these molecules with the oxophilic early-transition metals could give rise to MO^+ formation. Further, MO^+ may arise as a secondary product of further reactions of the primary MS^+ product. Therefore, a clear assignment of MO^+ formation in the FTICR to process 4 is difficult. Careful analysis of the FTICR data reveals that oxygen transfer to the metal cation is a primary process for Sc^+, $\phi(ScO^+) = 0.11 \pm 0.02$, whereas it is secondary for Ti^+ within the experimental uncertainty. The relative rates agree nicely with the GIB results (Tables 3 and 4), that is, $\sigma(ScS^+)/\sigma(ScO^+) = 3.3 \pm 0.9$ and $\sigma(TiS^+)/\sigma(TiO^+) = 10.9 \pm 2.6$ at ca. 0.03 eV. Further, the FTICR and GIB observations are consistent with the reaction enthalpies derived from Tables 1 and 2.

TABLE 4: Summary of Parameters in eq 1 Used for Fitting the Cross-sections and the Derived $D_0(Ti^+-S)$ in eV

reaction				E_0 (eV)[a]	σ_0	n	$D_0(Ti^+-S)$ (eV)
$COS + Ti^+$	→	$TiS^+ + CO$	(3)	<0	85 (15)[b]		>3.14 (0.01)
	→	$TiO^+ + CS$	(4)	<0	7.8 (1.3)[b]		
	→	$TiCO^+ + S$	(5)	2.57 (0.07)	0.92 (0.16)	0.7 (0.2)	
$CS_2 + Ti^+$	→	$TiS^+ + CS$	(9)	<0	200 (40)[b]		>4.50 (0.01)
	→	$TiCS^+ + S$	(10)	2.90 (0.05)	2.60 (0.27)	1.7 (0.1)	
$Xe + TiS^+$	→	$Ti^+ + S + Xe$	(12)	5.07 (0.31)	0.86 (0.31)	1.7 (0.2)	<5.07 (0.31)
$CO + TiS^+$ [c]	→	$TiO^+ + CS$	(14)	1.92 (0.28)	0.05 (0.03)	2.2 (0.2)	5.06 (0.29)
	→	$Ti^+ + CO + S$	(15)	5.28 (0.19)	0.50 (0.19)	1.8 (0.2)	<5.28 (0.19)
$CO_2 + TiS^+$	→	$TiO^+ + COS$	(19)	0.44 (0.12)	0.07 (0.02)	2.1 (0.2)	5.01 (0.14)
	→	$TiOS^+ + CO$	(20)	2.12 (0.15)	0.23 (0.05)	1.1 (0.2)	
	→	$TiO^+ + CO + S$	(21)	3.70 (0.27)	0.85 (0.33)	1.6 (0.2)	5.13 (0.27)
	→	$Ti^+ + S + CO_2$	(22)	5.14 (0.20)	0.51 (0.15)	1.7 (0.1)	<5.14 (0.20)
$COS + TiS^+$	→	$TiS_2^+ + CO$[d]	(24)	0.84 (0.10)	1.32 (0.28)	1.4 (0.2)	
	→	$TiO^+ + CS_2$	(25)	0.42 (0.17)	0.03 (0.01)	1.9 (0.2)	4.92 (0.19)
	→	$Ti^+ + S_2 + CO$	(26)	3.45 (0.31)	0.60 (0.29)	1.8 (0.2)	4.67 (0.31)
	→	$TiO^+ + CS + S$	(28)	5.02 (0.42)	0.22 (0.12)	1.6 (0.2)	5.02 (0.43)
$D_2O + TiS^+$	→	$TiO^+ + D_2S$	(2)		87 (9)[b]		4.74 (0.07)
$D_2S + TiO^+$	→	$TiS^+ + D_2O$	(2′)		1.0 (0.5)[b]		
				≤0.10	0.031 (0.006)	0.15 (0.11)	≥4.74

[a] The E_0 values are the average of several threshold fits with uncertainties of one standard deviation. [b] Maximum cross-sections at $E_{CM} \approx 0.03$ eV in units of 10^{-16} cm^2. [c] The cross-section between 2.0 and 5.5 eV is attributed to reaction 13 and can be reproduced using $E_0 = 1.34 \pm 0.37$ eV, $\sigma_0 = 0.08 \pm 0.04$, and $n = 1.6 \pm 0.2$ (see text). [d] Fitting parameters for the endothermic feature after subtraction of exothermic part (see text).

Reactions of M^+ with CS_2. The reactions of bare M^+ (M = Sc, Ti) with CS_2 under GIB conditions (Figure 2) result in formation of two major products, the metal sulfide (MS^+) and the metal thiocarbonyl cations (MCS^+) according to reactions 9 and 10, respectively. Formation of MS_2^+ is observed as a minor channel for both Sc^+ and Ti^+ with magnitudes $<10^{-17}$ cm^2, and is not pursued any further.

$$M^+ + CS_2 \rightarrow MS^+ + CS \quad (9)$$

$$\rightarrow MCS^+ + S \quad (10)$$

The cross-sections obtained for the reactions of bare Sc^+ and Ti^+ with CS_2 exhibit similar energy dependencies. Both MS^+ cross-sections (M = Sc, Ti) show the typical behavior of exothermic processes (Tables 3 and 4). In contrast to the reactions with COS, the cross-sections for formation of ScS^+ and TiS^+ both match the LGS model (solid lines in Figure 2, $\alpha_{CS2} = 8.74$ Å^3)[31] at energies below 0.3 eV. Above 0.3 eV the cross-sections deviate from σ_{LGS} and tend toward a ca. E^{-1} dependence. Starting between 1.5 and 2.0 eV, the MS^+ cross-sections flatten out, a behavior that again is attributed to the formation of excited states of the product ions.

Formation of the metal-thiocarbonyl cations is endothermic for both metals (Figure 2). Analysis of the MCS^+ cross-sections using eq 1 yields thresholds of 3.12 ± 0.07 eV and 2.90 ± 0.05 eV for $ScCS^+$ and $TiCS^+$, respectively (Tables 3 and 4), which are converted to $D_0(Sc^+-CS) = 1.38 \pm 0.08$ eV and $D_0(Ti^+-CS) = 1.60 \pm 0.06$ eV. In a strict sense, these D_0 values may only be regarded as lower limits because of competition with the efficient reaction 9.[11f] The MCS^+ cross-sections peak near 4.5 eV where dissociation of the MCS^+ products becomes feasible, according to reaction 11.

$$M^+ + CS_2 \rightarrow MCS^+ + S \rightarrow M^+ + S + CS \quad (11)$$

The exothermicity of reaction 9 enables its examination by FTICR. Similar to the observations in the M^+/COS systems (M = Sc, Ti), both metals exhibit exothermic formations of MS^+ as the major processes with reaction rates of $k(ScS^+) = (7.7 \pm 1.5) \times 10^{-10}$ cm^3 molecule^{-1} s^{-1} and $k(TiS^+) = (7.6 \pm 1.5) \times 10^{-10}$ cm^3 molecule^{-1} s^{-1}, that is, $\phi(MS^+) = 0.60 \pm 0.12$ for both metals. Again, the corresponding MO^+ ions are formed in secondary reactions with background contaminants.

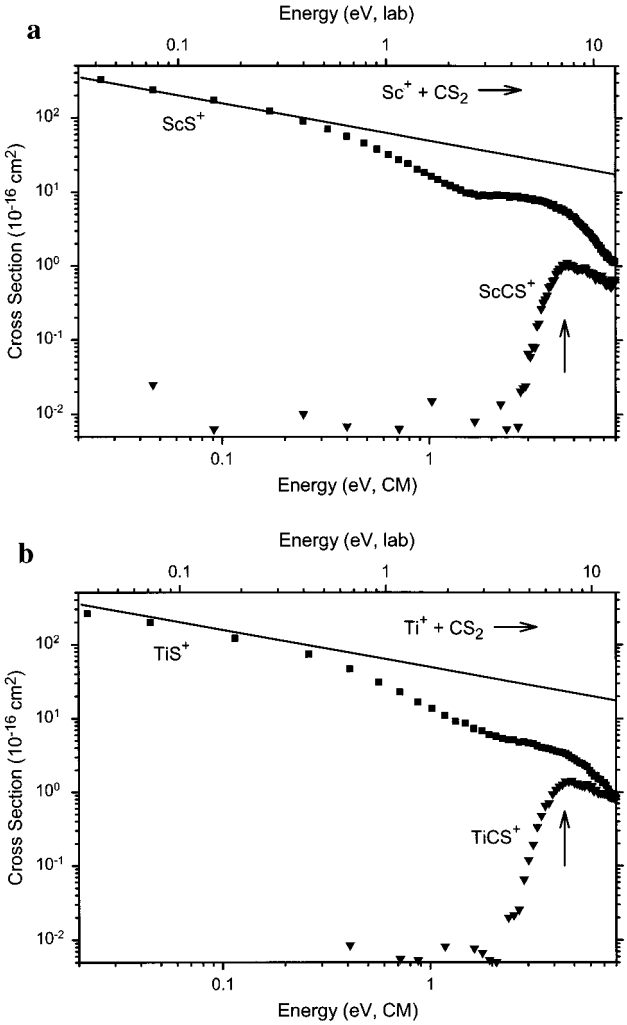

Figure 2. Product cross-sections for the reactions of M^+ (part a, M = Sc; part b, M = Ti) with CS_2 to form MS^+ (■) and MCS^+ (▼) as functions of E_{CM} (lower axis) and E_{lab} (upper axis). The arrow marks $D_0(S-CS) = 4.50$ eV. The solid lines represent σ_{LGS}.

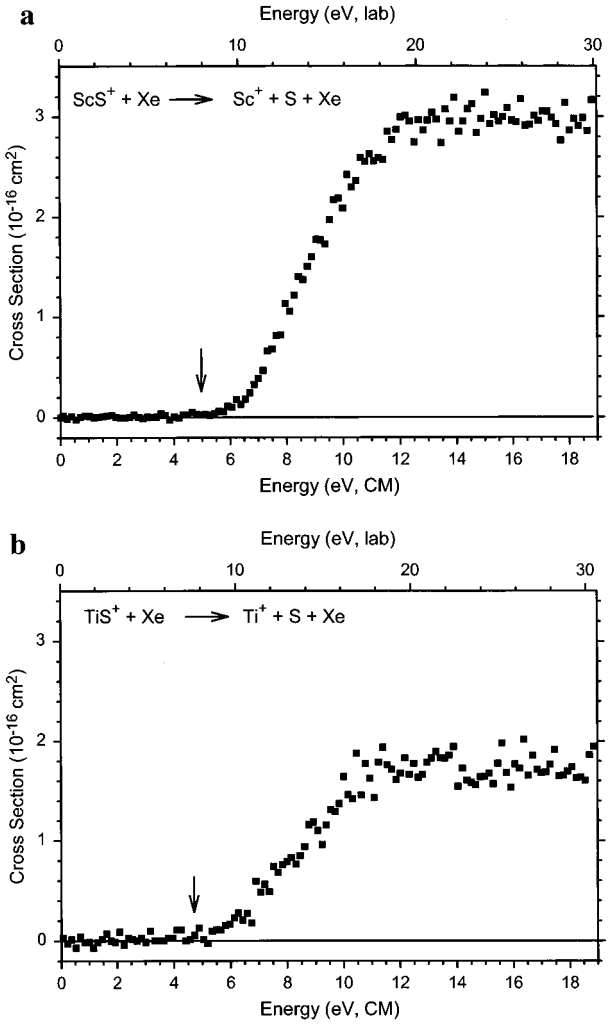

Figure 3. Cross-sections for the CID processes of MS^+ (part a, M = Sc; part b, M = Ti) with xenon to form M^+ (■) as functions of E_{CM} (lower axis) and E_{lab} (upper axis). The arrows mark $D_0(Sc^+-S) = 4.97$ and $D_0(Ti^+-S) = 4.74$ eV. The data for M = Ti is more scattered because of the overlap with the Ar_2^+ dimer (see Experimental Section).

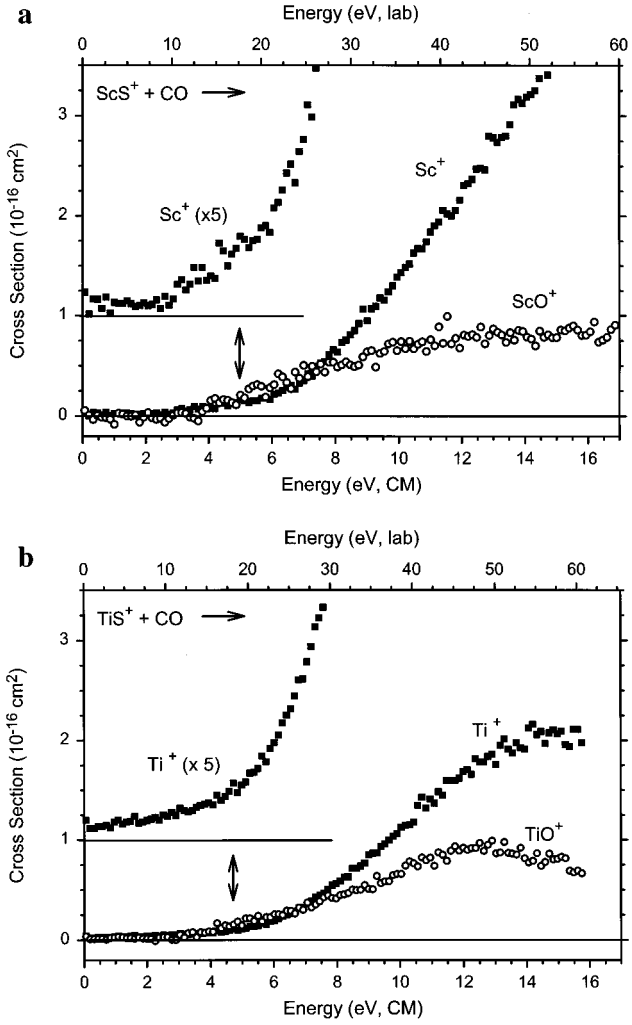

Figure 4. Product cross-sections for the reactions of MS^+ (part a, M = Sc; part b, M = Ti) with CO to form M^+ (■) and MO^+ (○) as functions of E_{CM} (lower axis) and E_{lab} (upper axis). The insets show the threshold regions of the M^+ cross-sections on expanded vertical scales and offset from zero by 1×10^{-16} cm^2. The arrows mark $D_0(Sc^+-S) = 4.97$ and $D_0(Ti^+-S) = 4.74$ eV.

Reaction of MS^+ with Xe. The MS^+ ions are generated in the flow tube by addition of small amounts of COS. To probe the purity of the MS^+ (M = Sc, Ti) beams, the mass-selected ions are collided with xenon. Apart from the Ar_2^+ problem mentioned above, the most severe impurities are the corresponding metal dioxide cations MO_2^+, which are isobaric with MS^+. Formation of MO^+ accompanied by loss of an oxygen atom is considered characteristic for the dioxo species.[35,36] The cross-sections for MO^+ (M = Sc, Ti) are below 0.1×10^{-16} cm^2, and hence we conclude that the MS^+ ion beams comprise only trace amounts of the metal dioxide cations if any at all.

$$MS^+ + Xe \rightarrow M^+ + S + Xe \qquad (12)$$

The only product of the reaction of MS^+ (M = Sc, Ti) with xenon is M^+ formed in the CID reaction 12. Threshold analysis of the M^+ cross-sections (Figure 3) with eq 1 yields 5.74 ± 0.26 eV and 5.07 ± 0.31 eV for Sc^+ and Ti^+, respectively. Both values exceed $D_0(S-CO) = 3.140 \pm 0.005$ eV and $D_0(S-CS) = 4.50 \pm 0.04$ eV, in agreement with the exothermic behavior observed for reactions 3 and 9. These thresholds obtained from the CID measurements can be regarded as rigorous upper limits[17a,37] for $D_0(M^+-S)$.

Reactions of MS^+ with CO. Figure 4 shows the cross-sections obtained when MS^+ ions are reacted with CO in the GIB instrument. Two major products, M^+ and MO^+, are formed and can be assigned to reactions 13, 14, and 15. At higher energies, formation of the metal carbides according to reaction 16 occurs as an inefficient side reaction, $\sigma_{max} = 0.2 \times 10^{-16}$ cm^2. This latter reaction is not shown in Figure 4 nor discussed further.

$$MS^+ + CO \rightarrow M^+ + COS \qquad (13)$$

$$\rightarrow MO^+ + CS \qquad (14)$$

$$\rightarrow M^+ + S + CO \qquad (15)$$

$$\rightarrow MC^+ + SO \qquad (16)$$

ScS^+ and TiS^+ show similar reactivity patterns with CO in that M^+ and MO^+ formations compete efficiently at low energies, whereas formation of M^+ prevails at higher energies (Figure 4). A closer look at the low-energy parts of the M^+ cross-sections (Figure 4, expansions) indicates that these result from more than one process. The Sc^+ cross-section has a small exothermic tail, starts to rise near 2.5 eV, and rises more rapidly

at about 5.5 eV. The cross-section of Ti^+ starts with a slight vertical offset (0.02×10^{-16} cm^2), rises smoothly up to 5.0 eV, and then rises more sharply. The high-energy parts of both M^+ cross-sections can be safely attributed to the CID process (reaction 15), because the only other possible high-energy process would be complete dissociation into the elements (reaction 17), which has its threshold 11.109 eV = D_0(C−O) above reaction 15.

$$MS^+ + CO \rightarrow M^+ + S + C + O \qquad (17)$$

Subtraction of the low-energy features and analysis of the remaining cross-sections with eq 1 leads to thresholds of $E_0(Sc^+) = 5.92 \pm 0.18$ eV and $E_0(Ti^+) = 5.28 \pm 0.19$ eV for CID. Both thresholds exceed those from CID with Xe in good agreement with earlier observations for collisional activation of metal-sulfide cations by CO.[10a] Analysis of the low-energy part of the M^+ cross-section is made difficult because of the small energy range, the low intensities, and the additional features at energies below 2 eV. The threshold analysis of the Sc^+ cross-sections between 2.0 and 5.5 eV with eq 1 is conducted by two approaches: (i) the small exothermic tail is subtracted before analysis leading to an upper limit of $E_{0,i}(Sc^+) = 2.66 \pm 0.23$ eV or (ii) the part of the cross-section between 2.5 and 5.5 eV is fitted without subtraction of the exothermic tail resulting in a lower limit of $E_{0,ii}(Sc^+) = 1.79 \pm 0.49$ eV. Averaging these limits, we arrive at $E_0(Sc^+) = 2.10 \pm 0.80$ eV (Table 3). Together with the thermochemistry given in Tables 1 and 2, we arrive at $D_0(Sc^+-S) = 5.24 \pm 0.80$ eV. Thus, the assignment of $E_0(Sc^+)$ to reaction 13 seems reasonable. For M = Ti, the analysis of the M^+ cross-section in the low-energy region is hampered by the vertical offset. With use of $E_0 = 1.34 \pm 0.37$ eV, $\sigma_0 = 0.08 \pm 0.04$, and $n = 1.6 \pm 0.2$, the cross-section between 2.0 and 5.5 eV is well reproduced. This leads to $D_0(Ti^+-S) = 4.48 \pm 0.37$ eV.

The interesting question remaining concerns the assignment of the exothermic tail in the Sc^+ cross-section and the origin of the vertical offset in the Ti^+ cross-section to chemical processes. Because reactions 13−17 cannot account for these features, processes involving molecules other than CO and MS^+ need to be considered. Despite our effort to avoid O_2 leakage, it is possible that small amounts of O_2 enter the reaction cell when CO is introduced, and likewise MO_2^+ is the only impurity that cannot be removed efficiently from the MS^+ beam by mass selection. Of the possible reactions involving traces of MO_2^+ and/or O_2, the only one that could lead to the low-energy features observed is reaction 18.

$$MS^+ + O_2 \rightarrow M^+ + SO_2 \qquad (18)$$

Using the thermochemistry of Tables 1 and 2, we calculate that $\Delta_R H(18) = D_0(M^+-S) - 5.922 \pm 0.005$ eV. According to the upper bounds of $D_0(M^+-S) < 5.74 \pm 0.26$ eV and 5.07 ± 0.31 eV for Sc^+ and Ti^+, respectively, derived from the CID of MS^+ with Xe, reaction 18 is exothermic.

The second process observed in the MS^+/CO system is formation of MO^+ with $E_0(ScO^+) = 3.70 \pm 0.27$ eV and $E_0(TiO^+) = 1.92 \pm 0.28$ eV (Tables 3 and 4). The larger uncertainties in these thresholds can be attributed to the small magnitudes, $\sigma_{max}(ScO^+)$ and $\sigma_{max}(TiO^+) = 10^{-16}$ cm^2, and the slow rises of the MO^+ cross-sections. Using these E_0 values, we arrive at $D_0(Sc^+-S) = 7.10 \pm 0.28$ eV and $D_0(Ti^+-S) = 5.06 \pm 0.29$ eV. Both values exceed the upper limits derived from CID of MS^+ with Xe, thus pointing to barriers en route to formation of MO^+ as found in the analogous VS^+/CO system.[10a]

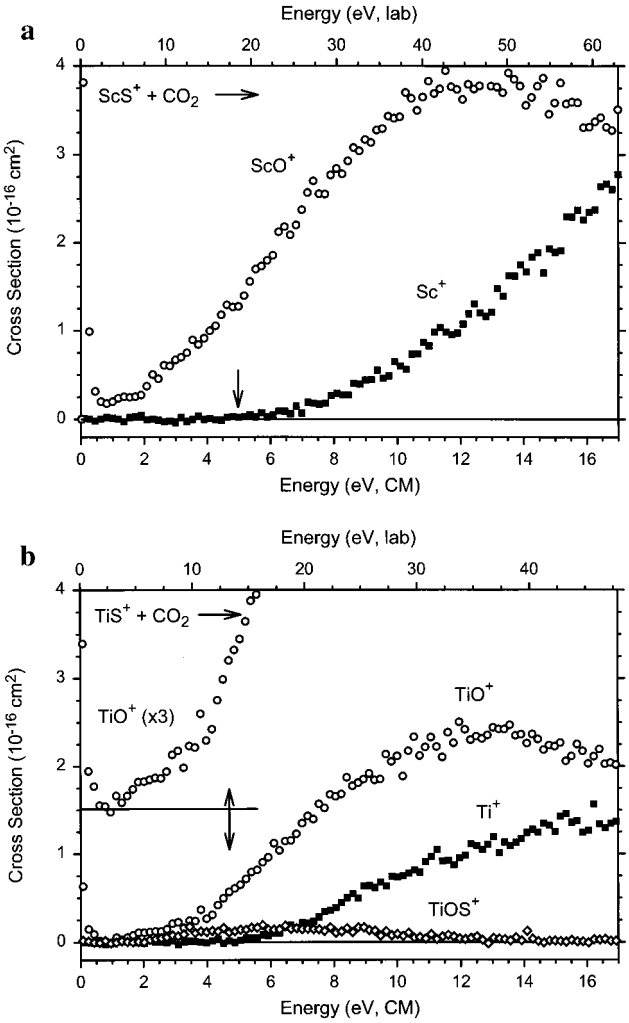

Figure 5. Product cross-sections for the reactions of MS^+ (part a, M = Sc; part b, M = Ti) with CO_2 to form MO^+ (○), M^+ (■), and MOS^+ (◇) as functions of E_{CM} (lower axis) and E_{lab} (upper axis). The inset in (part b) shows the threshold region of the TiO^+ cross-section on an expanded vertical scale and offset from zero by 1.5×10^{-16} cm^2. The arrows mark $D_0(Sc^+-S) = 4.97$ and $D_0(Ti^+-S) = 4.74$ eV.

Reactions of MS^+ with CO_2. The reactions of MS^+ with CO_2 (Figure 5) lead to M^+, MO^+, and MOS^+ products, which can be attributed to reactions 19−22.

$$MS^+ + CO_2 \rightarrow MO^+ + COS \qquad (19)$$

$$\rightarrow MOS^+ + CO \qquad (20)$$

$$\rightarrow MO^+ + S + CO \qquad (21)$$

$$\rightarrow M^+ + S + CO_2 \qquad (22)$$

In contrast to the reactions of MS^+ with CO, formation of MO^+ dominates the observed energy range when MS^+ is reacted with CO_2. This observation can be attributed mainly to the lower C−O bond energy in CO_2 (5.453 ± 0.002 eV) compared with CO (11.109 ± 0.005 eV). On first sight, Sc^+ and Ti^+ seem to show again a similar behavior. Closer inspection reveals that the ScO^+ cross-section consists of an exothermic tail and an obvious endothermic feature, whereas the TiO^+ cross-section exhibits an additional change in slope near 3.5 eV. Analysis of the TiO^+ cross-section after subtraction of the exothermic tail, which can be attributed to the presence of residual O_2 (see

above), leads to $E_0(TiO^+) = 0.44 \pm 0.12$ eV and 3.70 ± 0.27 eV (Table 4). Using the thermochemistry given in Tables 1 and 2, we can assign theses thresholds to reactions 19 and 21, an assignment further supported by the fact that the threshold difference of $\Delta E_0 = 3.26 \pm 0.30$ eV is consistent with $D_0(S-CO) = 3.14$ eV, the energy difference between reactions 19 and 21. The thresholds measured correspond to $D_0(Ti^+-S) = 5.01 \pm 0.14$ and 5.13 ± 0.27 eV, respectively. Because both reactions 19 and 21 are observed for M = Ti, there is no obvious reason only one process should take place in M = Sc. Analysis of the cross-section with eq 1 over several energy ranges (0.55−12.0 eV) reveals that the threshold of $E_0(ScO^+) = 0.77 \pm 0.08$ eV can be attributed to the low-energy path, reaction 19, and leads to $D_0(Sc^+-S) = 5.60 \pm 0.10$ eV. At higher energies, reaction 21 also contributes to the cross-section, but is not sufficiently distinct for M = Sc to allow unambiguous evaluation of the threshold.

Measurement of the reverse reaction 23 with FTICR is a suitable way to prove the assignment of the low-energy thresholds to reaction 19, because it should be exothermic for M = Sc and Ti according to the above-derived thresholds.

$$MO^+ + COS \rightarrow MS^+ + CO_2 \qquad (23)$$

Trapping MO^+ (M = Sc, Ti) cations in COS leads to exclusive formation of MS^+ as primary products with reaction efficiencies of 0.04 ± 0.01 and ca. $(1.0 \pm 0.2) \times 10^{-5}$ for M = Sc and Ti, respectively. The observation that both metal sulfide cations are formed under FTICR conditions is consistent with the GIB results and thus strengthens the assignments made above.

The other major channel observed when MS^+ is reacted with CO_2 in the GIB instrument corresponds to the CID process (reaction 22). The thresholds obtained upon analysis with eq 1 are $E_0 = 5.64 \pm 0.37$ eV and 5.14 ± 0.20 eV for Sc^+ and Ti^+, respectively (Tables 3 and 4). As mentioned above for CID with CO and Xe, these thresholds are upper limits for $D_0(M^+-S)$. The large uncertainties can be attributed to the slow rise of the M^+ cross-sections, which cause the threshold analysis to be less accurate. In addition, inefficient formation of MOS^+ according to reaction 20 is observed as a third process for M = Ti. Analysis of the threshold gives $E_0 = 2.12 \pm 0.15$ eV, which leads to $D_0(STi^+-O) = 3.33 \pm 0.15$ eV.

Reactions of MS^+ with COS. Three products, MS_2^+, MO^+, and M^+, are formed when MS^+ (M = Sc, Ti) is reacted with COS in the GIB instrument. The observed cross-sections can be attributed to reactions 24−28.

$$MS^+ + COS \rightarrow MS_2+ + CO \qquad (24)$$

$$\rightarrow MO^+ + CS_2 \qquad (25)$$

$$\rightarrow M^+ + S_2 + CO \qquad (26)$$

$$\rightarrow M^+ + S + COS \qquad (27)$$

$$\rightarrow MO^+ + CS + S \qquad (28)$$

As observed for the other reactants, ScS^+ and TiS^+ show similar reactivity patterns in their reactions with COS. The cross-sections for formation of MS_2^+ increase with decreasing energy, and thus are exothermic, $\sigma(ScS_2^+) = 1 \times 10^{-16}$ cm^2 at $E_{CM} = 0.07$ eV vs $\sigma(TiS_2^+) = 8 \times 10^{-16}$ cm^2 at $E_{CM} = 0.09$ eV. The exothermic feature of the MS_2^+ cross-section is less pronounced for M = Sc. This observation can be rationalized easily by the different electronic properties of the metals involved. Scandium cation[38] has two unpaired electrons that are used to form bonds to the first S ligand. Addition of a second sulfur atom to ScS^+ requires partial breaking of the strong Sc^+-S bond. In contrast, titanium has one more electron that can be used for the second STi^+-S bond. Exothermic formation of MS_2^+ from MS^+ and COS results in a lower limit of $D_0(SM^+-S) > 3.140 \pm 0.005$ eV. Both cross-sections exhibit pronounced endothermic features starting near 1 eV. Analysis of endothermic features after subtraction of the exothermic parts yields $E_0(ScS_2^+) = 0.90 \pm 0.19$ eV and $E_0(TiS_2^+) = 0.84 \pm 0.10$ eV. These thresholds may be attributed to formation of MS_2^+ in different spin states or connectivities in analogy to the VS^+/COS system.[10a] However, to the best of our knowledge no thermochemical data are available for ScS_2^+ and TiS_2^+, thus, the exothermicity of process 24 is unknown and the determined thresholds can only serve as lower limits for the electronic state splittings and/or isomer stabilities.

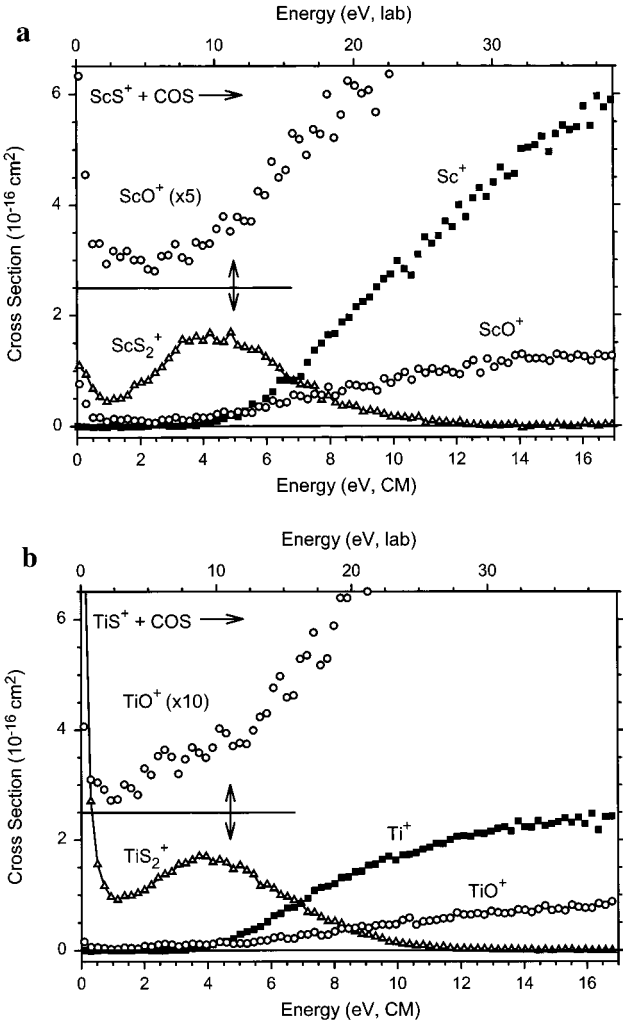

Figure 6. Product cross-sections for the reaction of MS^+ (part a, M = Sc; part b, M = Ti) with COS to form MS_2^+ (△), M^+ (■), and MO^+ (○) as a function of E_{CM} (lower axis) and E_{lab} (upper axis).

The other two products observed are MO^+ and M^+, formed in the endothermic reactions 25−28. Although formation of MO^+ is the preferred process at lower energies, formation of M^+ is dominant for the high-energy region. Closer inspection of the MO^+ cross-sections reveals that ScS^+ and TiS^+ may show threshold behavior different from the situation found in the MS^+/CO_2 systems (see above). The small exothermic tail present in both MO^+ cross-sections can be attributed to presence of

TABLE 5: Bimolecular Rate Constants for $MS^+ + H_2O \rightleftarrows MO^+ + H_2S$[a] with M = Sc and Ti, Reaction Enthalpies $\Delta_R H_0$ for Reaction 2 and the Derived $D_0(M^+-S)$ in eV

		$k_{(2)}$[b]	$k_{(2')}$[b]	$\Delta_R H_0$[c]	$D_0(M^+-S)$
Sc	(FTICR)	6.2 ± 1.2 (25%)	0.021 ± 0.004 (0.16%)	−0.129 ± 0.025	5.01 ± 0.07
Sc	(GIB)	17 ± 4 (70%)	0.010 ± 0.005 (0.08%)	−0.174 ± 0.023	4.92 ± 0.06
Ti	(FTICR)	4.9 ± 1.0 (20%)	<0.02 ± 0.01 (0.13%)	<−0.124 ± 0.025	<4.75 ± 0.07
Ti	(GIB)	5.4 ± 1.1 (22%)	0.056 ± 0.022 (0.36%)	−0.100 ± 0.018	4.74 ± 0.07

[a] The deuterium analogues D_2O and D_2S are used in the GIB (see Experimental Section). [b] Rate constants k are given in 10^{-10} cm^3 molecule^{-1} s^{-1}. Values in parentheses are the reaction efficiencies ϕ according to the capture theory. [c] Derived via the Gibbs−Helmholtz equation and converted to 0 K using the calculated thermal corrections to enthalpy and entropy and assuming that the ions were equilibrated to 298 K.

residual O_2. Analysis of the MO^+ cross-sections with eq 1 leads to $E_0(ScO^+) = 1.22 \pm 0.39$ eV and $E_0(TiO^+) = 0.42 \pm 0.17$ eV as well as 5.02 ± 0.42 eV. Both low-energy thresholds can be assigned to reaction 25 and give rise to $D_0(Sc^+-S) = 5.98 \pm 0.40$ eV and $D_0(Ti^+-S) = 4.92 \pm 0.19$ eV. The second threshold of the TiO^+ cross-section, $E_0(TiO^+) = 5.02 \pm 0.42$ eV, is most likely caused by formation of TiO^+ according to reaction 28. The difference between processes 25 and 28 is the dissociation of CS_2 into CS and S, and the experimental threshold difference of 4.60 ± 0.45 eV for TiO^+ agrees well with $D_0(SC-S) = 4.50 \pm 0.04$ eV. For M = Sc, the occurrence of process 28 cannot be excluded, but similar to processes 19 and 21 in the ScS^+/CO_2 system, process 28 seems to be less efficient than process 25. Again, FTICR proves useful in providing information about the reverse of reaction 25. When MO^+ ions (M = Sc, Ti) are trapped with CS_2, exothermic formation of MS^+ occurs with efficiencies of 0.06 ± 0.01 and 0.003 ± 0.001, respectively, in good agreement with the above-assigned endothermicity of reaction 25.

The third process observed in the GIB experiments is formation of M^+, which dominates at higher energies. The measured thresholds at ca. 4.0 and 3.5 eV are lower than the lower limit of $D_0(M^+-S) > 4.50 \pm 0.04$ eV obtained from the exothermicity of reaction 9 for both metals, thus the CID process (reaction 27) can be excluded as the origin of M^+ formation at threshold. Another possible pathway to formation of M^+ involves abstraction of sulfur concomitant with generation of S_2 and CO according to reaction 26. This process is driven by formation of the strong S−S bond, $D_0(S-S) = 4.364 \pm 0.005$ eV. Note that formation of an intact COS_2 molecule as another possible neutral product is less likely than liberation of S_2 and CO.[10a] Although the CID process (reaction 27) does not contribute to the M^+ channels below 5.74 ± 0.26 and 5.07 ± 0.31 eV, respectively, it must be included in the fitting procedures to reproduce the entire cross-sections for the M^+ channels. This is achieved by subtracting varying amounts of a scaled Xe−CID cross-section from the original M^+ cross-section before analysis. The threshold energy is monitored with respect to this variation throughout a reasonable range in the amount of Xe−CID subtracted. This leads to average thresholds of $E_0(Sc^+) = 4.17 \pm 0.13$ eV and $E_0(Ti^+) = 3.45 \pm 0.31$ eV. Use of these thresholds and the assumption of S_2 and CO neutral products yields M^+-S bond energies of 5.39 ± 0.13 eV and 4.67 ± 0.31 eV for M = Sc and Ti, respectively.

Reactions of MX^+ with H_2Y (X,Y = O, S). The cross-sections obtained when MX^+ is reacted with D_2Y (X,Y = O, S) under GIB conditions are depicted in Figure 7. Here, the deuterated variants D_2O and D_2S are used to cope with the limited mass resolution of the quadrupole analyzer. MS^+ and MO^+ (M = Sc and Ti) are the only significant products formed at low energies (below 1 eV) and can be assigned to reaction 2 and its reverse (2′). As is obvious from the cross-sections shown in Figures 7a and 7b, formation of both MO^+ and MS^+ (M = Sc, Ti) is observed at low energies. Thus, the S/O exchange

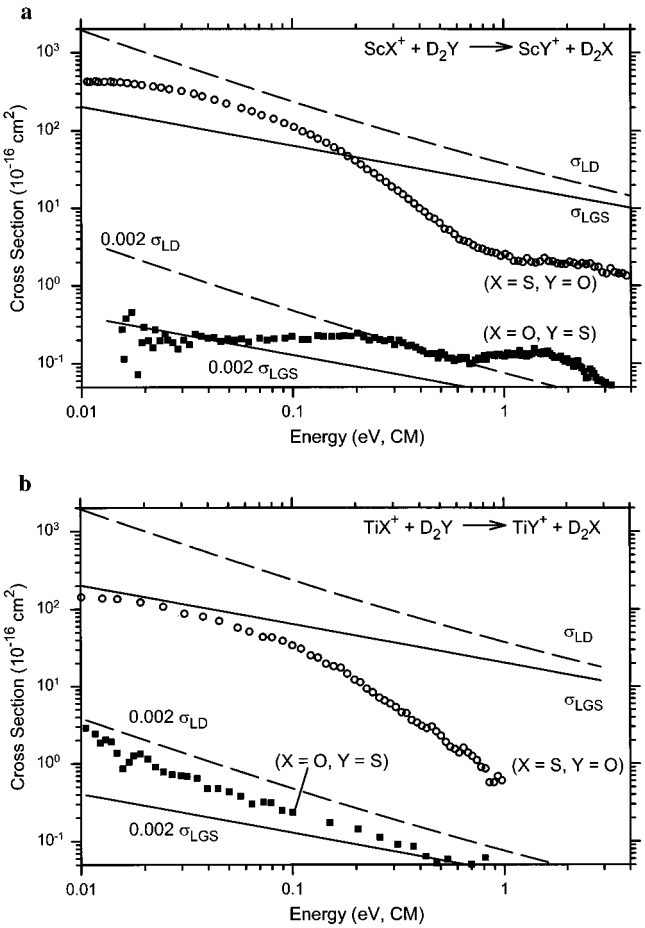

Figure 7. Product cross-sections for the reactions of MS^+ (part a, M = Sc; part b, M = Ti) with D_2O to form MO^+ (○) and MO^+ (part a, M = Sc; part b, M = Ti) with D_2S to form MS^+ (■) as functions of the center-of-mass energies (E_{CM}, lower axis) and laboratory energies (E_{lab}, upper axis). The solid and dashed lines represent σ_{LGS} and $\sigma_{locked\ dipole}$, respectively.

according to reactions 2 and 2′ is almost thermoneutral, and the qualitative assignment of endo- or exothermic behavior is difficult. Instead, the ratio of the rate constants can be used for the determination of $D_0(M^+-S)$ via $K_{eq}(2) = k_{(2)}/k_{(2')}$. At $E_{CM} = 0.03$ eV, the data in Figure 7 correspond to MO^+ cross-sections of $\sigma(ScO^+) = (323 \pm 65) \times 10^{-16}$ cm^2 and $\sigma(TiO^+) = (87 \pm 17) \times 10^{-16}$ cm^2, whereas the MS^+ cross-sections are $\sigma(ScS^+) = (0.20 \pm 0.06) \times 10^{-16}$ cm^2 and $\sigma(TiS^+) = (1.0 \pm 0.5) \times 10^{-16}$ cm^2. Using eq 29, we arrive at the rate constants for $k_{(2),GIB}$ and $k_{(2'),GIB}$ listed in Table 5.

$$k\langle E_0\rangle = (2E_0/\mu)^{0.5}\,\sigma(E_0) \qquad (29)$$

The reaction rates are converted to $\Delta_R H_0$ values of -0.174 ± 0.023 and -0.100 ± 0.018 eV for M = Sc and Ti, respectively, by means of $\Delta_R G_{298} = -RT\ \ln(k_{(2)}/k_{(2')})$ and

$\Delta(\Delta_R G_{298} - \Delta_R G_0) = -0.017 \pm 0.001$ eV obtained at the B3LYP/6-311+G* level of theory.[9] Using the thermochemical data given in Tables 1 and 2, we arrive at $D_0(Sc^+-S) = 4.92 \pm 0.06$ eV and $D_0(Ti^+-S) = 4.74 \pm 0.07$ eV. Given these results, we can analyze the cross-sections for reaction 2′ using eq 1. Good fits of the data in the Sc system are achieved, whereas the analysis of the Ti data is more difficult. Conservatively, we arrive at the parameters listed in Tables 3 and 4. Note that the thresholds obtained are in excellent agreement with the results of the equilibrium assumptions. These thresholds correspond to bond energies of $D_0(ScS^+) = 4.92 \pm 0.07$ eV and $D_0(TiS^+) \geq 4.74 \pm 0.07$ eV.

The rates of reaction 2 and its reverse (2′) are also measured under FTICR conditions. Formation of MO^+ is observed upon trapping of MS^+ (M = Sc, Ti) in water. To distinguish between the reaction of MS^+ with background O_2 and H_2O, ^{18}O-labeled water was used as reagent. Analysis of the kinetic data yields $k_{(2),FTICR}(ScO^+) = (6.2 \pm 1.2) \times 10^{-10}$ cm^3 molecule^{-1} s^{-1} and $k_{(2),FTICR}(TiO^+) = (4.9 \pm 1.0) \times 10^{-10}$ cm^3 molecule^{-1} s^{-1} (Table 5). The reverse reaction (i.e., $MO^+ + H_2S$) results in formation of ScS^+ for M = Sc, whereas no formation of TiS^+ is observed even after trapping of TiO^+ cations in 0.8×10^{-4} mTorr H_2S for 160 s. From the former experiment, a rate constant of $k_{(2'),FTICR}(ScS^+) = (0.021 \pm 0.004) \times 10^{-10}$ cm^3 molecule^{-1} s^{-1} is derived (Table 5). For titanium, reaction 2′ may not have been observed because of the fast back-reaction of TiS^+ with residual water, reaction 2, which is present in the background.[39] To check the relevance of this possibility, additional FTICR experiments were performed which involved the simultaneous isolation of TiO^+ cations with two different Ti isotopes, $m/z(^{48}Ti^{16}O^+) = 64$ and $m/z(^{50}Ti^{16}O^+) = 66$. The isolated cations are reacted with H_2S to give $^{48}Ti^{32}S^+$ and $^{50}Ti^{32}S^+$. Again, neither $m/z = 80$ nor 82 are observed after 70 s using $p_{H_2S} = 5 \times 10^{-5}$ mTorr. Next, the experiment is repeated as a double-resonance (DR) experiment,[40] in which $^{48}Ti^{32}S^+$ is continuously ejected from the cell throughout the entire reaction time. An upper limit of $k_{(2'),FTICR}(TiS^+) \leq (0.02 \pm 0.01) \times 10^{-10}$ cm^3 molecule^{-1} s^{-1} is derived from these DR experiments. $\Delta_R H_0$ values of -0.129 ± 0.025 and $\leq -0.124 \pm 0.025$ eV are obtained for M = Sc and Ti, respectively, by use of the above-derived FTICR reaction rates. Despite the small $\Delta_R H_0$ value for M = Sc, all attempts to establish an equilibrium failed, because of the low rates for ScS^+ formation as well as reactions with background water and oxygen. Combined with the thermochemistry in Table 1, the FTICR data result in $D_0(ScS^+) = 5.01 \pm 0.07$ eV and an upper limit of $D_0(TiS^+) \leq 4.75 \pm 0.07$ eV.

Computational Findings. It is important to know the nature of the electronic states of the MS^+ species to understand these experimental results. DFT calculations were used to establish this information. At the ADF/BP level of theory (Table 6), we find low-spin $^1\Sigma^+$ and $^2\Delta$ ground states for ScS^+ and TiS^+, respectively. These states result from the perfect pairing of Sc^+ (^{3}D)[38] and Ti^+ (^{4}F)[38] with S (^{3}P)[41] yielding $(1\sigma)^2(2\sigma)^2(1\pi)^4$ and $(1\sigma)^2(2\sigma)^2(1\pi)^4(1\delta)^1$ valence configurations, respectively. The $^1\Sigma^+$ ground state for scandium sulfide agrees with earlier calculations at the MCSCF level of theory.[42] The next higher states are the four triplet states at 2.18, 2.30, 2.75, and 2.94 eV with $^3\Pi/^3\Phi$, $^3\Pi/^3\Phi$, $^3\Sigma^+$, and $^3\Delta$ symmetry formed by excitation of a single electron from the 1π orbital into the 1δ or 3σ orbital ($^3\Pi/^3\Phi$) or from the 2σ into the 3σ or 1δ orbital ($^3\Sigma^+/^3\Delta$). Interestingly, Tilson and Harrison[42a] report only the $^3\Sigma^+$ and $^3\Delta$ as the lowest excited states at the MCSCF level of theory. Further, the state ordering is reversed with the $^3\Delta$ state at 2.45 eV because it is 0.3 eV more stable than the $^3\Sigma^+$ state. The reversed order most likely results from failure to treat correlation energy in the DFT approach used here. The lowest quintet state ($^5\Pi$) of ScS^+ has a $(1\sigma)^2(2\sigma)^2(1\pi)^2(1\delta)^1(3\sigma)^1$ configuration and is located at 4.45 eV. Not surprisingly, the splitting is much closer for the titanium sulfide cation with an extra electron in the nonbonding δ-manifold. The lowest excited state is TiS^+ ($^2\Sigma^+$) at 0.65 eV and involves the excitation of the uncoupled electron from the 1δ to the 3σ orbital. The lowest quartet states (both with $^4\Pi/^4\Phi$ symmetry) are formed by excitation of one electron from one of the doubly occupied 1π orbitals into either the empty 3σ or 1δ orbitals requiring 1.85 and 1.98 eV, respectively. We choose not to report theoretical bond energies because the ADF program used is not designed to assess accurate bond energies.

TABLE 6: State Splittings in eV and Bond Lengths *r* in Å for MS^+ (M = Sc, Ti) at the ADF/BP86 Level of Theory

E_{rel}	ScS^+ state	*r*	E_{rel}	TiS^+ state	*r*
0.00	$^1\Sigma^+$	2.096[a]	0.00	$^2\Delta$	2.056[b]
2.18	$^3\Pi/^3\Phi$[c]	2.299	0.65	$^2\Sigma^+$	2.030
2.30	$^3\Pi/^3\Phi$[c]	2.339	1.19	$^2\Pi/^2\Phi$[c]	2.082
2.75	$^3\Sigma^+$	2.197	1.85	$^4\Pi/^4\Phi$[c]	2.247
2.94	$^3\Delta$	2.248	1.98	$^4\Pi/^4\Phi$[c]	2.266
4.45	$^5\Pi$	2.736	2.23	$^4\Delta$	2.309

[a] Reoptimization at the B3LYP/6-311+G* level of theory yields $r = 2.087$ Å and $\nu = 618$ cm^{-1}. [b] Reoptimization at the B3LYP/6-311+G* level of theory yields $r = 2.039$ Å and $\nu = 610$ cm^{-1}. [c] A differentiation between Π and Φ states is not possible in the ADF/BP86 method used.

Discussion

The discussion is organized in the following way. First, brackets for $D_0(Sc^+-S)$ and $D_0(Ti^+-S)$ are derived from the reactions of M^+ with COS/CS_2 and CID of MS^+ (M = Sc, Ti). Next, these brackets are compared with the D_0 values obtained from the $MS^+ + COX$ (M = Sc, Ti; X = no atom, O, S) experiments performed with the GIB instrument. Further, independent $D_0(M^+-S)$ values are derived from reaction 2 and its reverse (2′) measured under GIB and FTICR conditions. Comparison of all data obtained leads to the recommended values for $D_0(Sc^+-S)$ and $D_0(Ti^+-S)$. Finally, $D_0(Sc^+-CS)$, $D_0(Ti^+-CS)$, and $D_0(STi^+-O)$ are briefly addressed.

Brackets. The exothermic behaviors of reactions 3 and 9 allow us to assign lower limits of 3.140 ± 0.005 and 4.50 ± 0.04 eV, respectively, on $D_0(M^+-S)$. Upper limits of $D_0(Sc^+-S) < 5.74 \pm 0.26$ and $D_0(Ti^+-S) < 5.07 \pm 0.31$ eV are obtained from the thresholds of CID with xenon. Within experimental error, comparable values are obtained for CID with CO_2. Using CO as a collision gas results in a higher threshold for the CID process than for xenon in line with the findings for the VS^+/CO system.[10a]

The efficiency of CID is influenced by the degrees of freedom, the mass, and the ion−molecule interactions of the collision gas.[10a] The latter can be estimated by comparing the M^+-CO and M^+-CO_2 complexation energies. Unfortunately, few experimental data (i.e., $D_0(Ti^+-CO) = 1.22 \pm 0.06$ eV)[34] are available in the literature. However, quantum chemical calculations at the CCSD(T) level of theory with atomic natural orbital basis sets predict $D_0(Sc^+-CO_2) = 0.90$ eV and $D_0(Ti^+-CO_2) = 0.92$ eV, $D_0(OSc^+-CO) = 0.88$ eV, and $D_0(OTi^+-CO) = 1.11$ eV.[42] Further, $D_0(Sc^+-CO) = 0.61$ eV and $D_0(Ti^+-CO) = 1.02$ eV have been obtained with all electron basis sets at the MCPF level of theory.[33] The complexation energies reveal that scandium interacts less strongly with CO

SCHEME 1

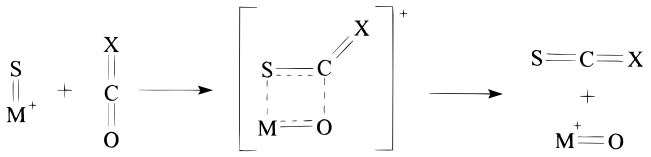

than with CO_2, whereas for M = Ti the two interactions are similar in energy. The strength of interaction influences the lifetime of the collision complex, that is, a weaker complexation results in a shorter lifetime. Thus, the M^+-CO complexes have shorter lifetimes in good agreement with the experimentally observed highest CID thresholds for CO. For the present purposes, the thresholds for M^+ formation in CID with xenon are used as upper limits for both metals, because atomic xenon is a more suitable CID gas than CO or CO_2 and no other process than dissociation contributes to formation of M^+ at threshold. Thus, we arrive at the following brackets for $D_0(M^+-S)$:

$$4.50 \pm 0.04\ (CS_2) < D_0(Sc^+-S) < 5.74 \pm 0.26\ (Xe)$$

$$4.50 \pm 0.04\ (CS_2) < D_0(Ti^+-S) < 5.07 \pm 0.31\ (Xe)$$

$MS^+ + COX$ (X = No Atom, O, S). Most of the remaining processes involve reactions of MS^+ with reagents leading to formation of M^+ and MO^+. In general, the reactions leading to MO^+ appear to be associated with kinetic restrictions, because their thresholds lead to $D_0(M^+-S)$ values which exceed those derived from the M^+ channel of the MS^+/COS couple and, in some cases, even those derived from CID (Tables 3 and 4). Existence of kinetic barriers can be rationalized by the involvement of four-centered transition structures en route to MO^+ (Scheme 1). A metathesis-like mechanism is conceivable, because ScS^+ and TiS^+ have low-lying empty orbitals capable of accepting π-electron density from the neutral. Upon occupation, these antibonding orbitals weaken the M^+-S bonds and may thus facilitate O/S exchange. Because higher oxidation states are not available for the early-transition metals, scandium and titanium, oxidative addition mechanisms are considered less likely for these metals.

The remaining thresholds for determination of $D_0(M^+-S)$ are those of reactions 13 and 26 for ScS^+ and reaction 26 for TiS^+. The two $D_0(Sc^+-S)$ values are consistent with one another, but the former reaction leads to a very imprecise bond energy. Therefore, our best GIB values are those obtained from reaction 26, $D_0(Sc^+-S) = 5.39 \pm 0.13$ eV and $D_0(Ti^+-S) = 4.67 \pm 0.31$ eV, which are consistent with the boundaries derived above. A drawback, however, is that these bond energies are derived from analysis of composite cross-sections for which the nature of the neutral is not characterized unambiguously in the experiments.

$MX^+ + H_2Y$ (X, Y = O, S). Comparison of the $D_0(M^+-S)$ values given in Tables 3−5 reveals that $D_0(Ti^+-S) = 4.67 \pm 0.31$ eV agrees within the uncertainties with the GIB (4.74 ± 0.07 eV) and FTICR ($\leq 4.75 \pm 0.07$ eV) data obtained for reaction 2 and its reverse. In contrast, $D_0(Sc^+-S) = 5.39 \pm 0.13$ eV derived from the threshold of reaction 26 is 0.47 and 0.38 eV higher than $D_0(Sc^+-S) = 4.92 \pm 0.06$ and 5.01 ± 0.07 eV obtained for reaction 2 and its reverse (2′) with GIB and FTICR, respectively.

There are two ways to rationalize the discrepancy for $D_0(Sc^+-S)$: (i) the M^+-S bond derived from the threshold of reaction 26 is overestimated because of the bimodal nature of the M^+ channel (see above) or (ii) the $D_0(Sc^+-S)$ value derived from reaction 2 is based on values that are too large for the equilibrium constant K_{eq}(reaction 2). The latter would result from either an underestimation of $k_{(2)}$ or an overestimation of $k_{(2')}$. For the FTICR data, an underestimation of $k_{(2),FTICR}$ can be excluded, because the reaction is rather fast and there is no obvious background component that would cause the regeneration of ScS^+ from ScO^+ resulting in a $k_{(2),FTICR}$ value that is too low. For similar reasons, overestimation of $k_{(2'),FTICR}$ is unlikely. Further, the formation of ScS^+ according to reaction 2′ has been studied at different pressure regimes. No ScS^+ signal is observed, at low substrate pressures, whereas, ScS^+ is indeed observed at the same reaction time but higher H_2S pressures. This finding suggests that excited ScO^+ ions are unlikely to be the source for ScS^+, because the higher H_2S pressures would result in more collisionally cooled ScO^+ ions. Assuming that excited states of ScO^+ react faster with H_2S to form ScS^+, the opposite effect should be observed. Further, the thermodynamic results for reaction 2 and its reverse (2′) from GIB and FTICR are in excellent agreement. Thus, reason i must be responsible for the deviation of the $D_0(Sc^+-S)$ values in that the threshold of process 26 is shifted to higher energies. This shift most likely results from the very strong Sc^+-S bond. The high $D_0(Sc^+-S)$ value renders formation of Sc^+ in the ScS^+/COS system strongly endothermic, $\Delta_R H_0(26) = 3.75 \pm 0.05$ eV with $D_0(Sc^+-S) = 4.97 \pm 0.05$ eV. This fact and the competition with more favorable channels such as reaction 24 causes the slow rise and low magnitude of the M^+ cross-section, which results in an elevated E_0 value for the M^+ channel leading to a slightly too large $D_0(Sc^+-S)$ derived for reaction 26.

Taking these considerations into account, we arrive at the final bond dissociation energies of $D_0(Sc^+-S) = 4.97 \pm 0.05$ eV, the average of the GIB and FTICR determinations from $K_{eq}(2)$, and $D_0(Ti^+-S) = 4.74 \pm 0.07$ eV, the GIB determination from $K_{eq}(2)$. In the next section, these bond energies are used in the discussion of the shapes and additional features of the exothermic MS^+ cross-sections observed in the reaction of M^+ with COS and CS_2 (Figures 1 and 2).

Electronic States. Using these D_0 values for M = Sc and Ti, $\Delta_R H_0 = -1.84 \pm 0.07$ eV and -1.58 ± 0.08 eV, respectively, are obtained for the sulfur-atom transfer from COS to M^+ in reaction 3. The ground states of the metal cations are Sc^+ (^{3}D) and Ti^+ (^{4}F).[38] Comparison of the state splittings in Table 6 with the $\Delta_R H_0$ values of reaction 3 reveals that for both metals only the formations of the spin-forbidden products, ScS^+ ($^1\Sigma^+$) and TiS^+ ($^2\Delta$, $^2\Sigma^+$, and $^2\Pi/^2\Phi$) are exothermic. This finding is in agreement with the deviation of the MS^+ cross-sections from σ_{LGS} as observed in the reactions of COS with Sc^+ (ca. $E^{-0.65}$) and Ti^+ (ca. $E^{-0.9}$). Likewise, the high-energy features of the ScS^+ and TiS^+ cross-sections can be attributed to the endothermic but spin-allowed formations of excited ScS^+ ($^3\Pi/^3\Phi$) and TiS^+ ($^4\Pi/^4\Phi$) starting near 0.5 and 0.3 eV, respectively. For sulfur transfer from CS_2, exothermic reactions of both metal ions yield only ground-state MS^+ product cations, which also implies spin inversion with CS_2. Both MS^+ cross-sections show LGS behavior at lowest energies and, even though S-atom abstraction from CS_2 is more energy-demanding than from COS, the former reagent shows larger efficiencies for both metals. We attribute this difference to the larger polarizability of CS_2 compared with COS (8.74 vs 5.71 Å^3)[31] as well as the presence of an additional sulfur atom which may contribute to spin−orbit coupling. Both effects may enhance the coupling between the spin surfaces and thereby increase the crossing probabilities with CS_2 compared with COS.

***D*$_0$(M$^+$−CS) and Δ$_f$*H*(TiOS$^+$).** In the reaction of M^+ with CS_2, the formation of MCS^+ according to reaction 10 is observed with thresholds of 3.12 ± 0.07 eV and 2.57 ± 0.07 eV for M = Sc and Ti. These thresholds are converted to $D_0(Sc^+-CS) = 1.38 \pm 0.08$ eV and $D_0(Ti^+-CS) = 1.60 \pm 0.06$ eV using the thermochemical data given in Tables 1 and 2. The MCS^+ ions are most likely thiocarbonyl complexes of the metal cations.[44] Comparison of the D_0 values for MCO^+ and MCS^+ (Table 1) shows that the CS ligand is bound more strongly to both metal cations. This observation agrees with the better σ-donor properties of CS because of its higher polarizability. Further, crystallographic data of mixed transition-metal complexes with CO and CS ligands[44] as well as theoretical studies[45] imply that the CS ligand is a better π-acceptor than CO. Comparison of $D_0(Sc^+-CS) = 1.38 \pm 0.08$ eV, $D_0(Ti^+-CS) = 1.60 \pm 0.08$ eV, $D_0(V^+-CS) = 1.70 \pm 0.08$ eV,[10a] and $D_0(Fe^+-CS) = 2.40 \pm 0.12$ eV[11f] indicates that the M^+-CS bonds strengthen with increasing number of electrons at the metal center, in good agreement with π-acceptor contribution to the bonding and with smaller ionic radii.

For the $TiOS^+$ species formed in reaction 20, $\Delta_f H_0(TiOS^+) = 9.04 \pm 0.18$ eV and $D_0(OTi^+-S) = 1.19 \pm 0.20$ eV are obtained using $D_0(STi^+-O) = 3.33 \pm 0.15$ eV, $D_0(Ti^+-O) = 6.88 \pm 0.07$ eV, and $D_0(Ti^+-S) = 4.74 \pm 0.07$ eV. Comparison of the Ti^+-S and Ti^+-O bonds in the mono- and bisligated species reveals that addition of S to TiO^+ results in a reduction of $D_0(Ti^+-O)$ by ca. 50%, whereas addition of O to TiS^+ reduces $D_0(Ti^+-S)$ to ca. 25%. The larger effect on addition of O can be rationalized by the higher electronegativity of oxygen compared with sulfur (3.50 vs 2.44).[45] Note however, that we have no structural information about the $TiOS^+$ species formed and cannot exclude the presence of an S−O bond in the ion.

Conclusions

A variety of reactions are examined to understand the reactivity of the early-transition metal sulfide cations, ScS^+ and TiS^+. The bond dissociation energies for these species, $D_0(Sc^+-S) = 4.97 \pm 0.05$ eV and $D_0(Ti^+-S) = 4.74 \pm 0.07$ eV, are derived principally from GIB and FTICR studies of the equilibrium of reaction 2. The accuracy of these values is verified by comparison with the results for several formation and degradation reactions examined with the GIB and FTICR techniques. We further determine the bond dissociation energies for M^+-CS from the thresholds of reaction 10. This yields $D_0(Sc^+-CS) = 1.38 \pm 0.08$ eV and $D_0(Ti^+-CS) = 1.60 \pm 0.08$ eV, which are substantially weaker than comparable bond energies for late-transition metal ions. Finally, we derive the heat of formation for $TiOS^+$, 9.04 ± 0.18 eV, from the threshold for reaction 20.

Several potential routes to determining the M^+-S bond dissociation energies are explored in this work, and a detailed assessment of the utility of these routes is made. As with the corresponding metal oxides,[47,48] the quantitative assessment of the absolute bond dissociation energies using mass spectrometric techniques is much more difficult to achieve for the early-transition metals, when compared with the later members of the 3d series.[9−11] The major reason is the enormous bond strengths of these metals, which limits the choices of volatile targets XS used in endothermic sulfur-atom transfer reactions to those having larger X−S bond strengths than the metals. Indeed, the only simple, small target molecules that meet this criterion for scandium, $D_0(Sc^+-S) = 4.97 \pm 0.05$ eV, are species such as sulfur monoxide, $D_0(O-S) = 5.35 \pm 0.02$ eV, or thioformaldehyde, $D_0(H_2C-S) \approx 6.0$ eV,[49] which are not available as bulk compounds that can be used as neutral reagents in GIB or FTICR measurements. Moreover, the large bond strengths are likely to impose barriers in excess of the reaction endothermicities on the reactions observed leading to erroneous assignments of the experimental thresholds as found for the processes involving MO^+ formation. Similarly, assessment of $D_0(M^+-S)$ via thermochemical cycles using $D_0(M-S)$ and IE(MS) is made difficult, because the corresponding IEs are probably low, thereby limiting the prospects of charge-transfer bracketing experiments. For example, combination of $D_0(Sc^+-S) = 4.97 \pm 0.05$ eV, IE(Sc) = 6.562 eV,[38] and $D_0(Sc-S) = 4.93 \pm 0.13$ eV[4] implies IE(ScS) = 6.52 ± 0.14 eV. Thus, charge-transfer bracketing would involve substrates such as aromatic amines or metallocenes for which other pathways, for example, association, are likely to compete. Although ICR studies can provide complementary information, these are mostly limited to relative energetics and are thus based on reference values. In the present work, the reference species are the metal oxides, ScO^+ and TiO^+, where similar problems in determining the absolute bond strengths apply. We note, however, that the low IEs of ScS and TiS suggest these molecules should be attractive candidates for precise IE measurements using photoionization techniques.

Acknowledgment. This research was supported by the Deutsche Forschungsgemeinschaft, the Volkswagen-Stiftung, the Fonds der Chemischen Industrie (scholarship for I.K.), and the National Science Foundation, CHE-9877162. The Konrad Zuse Zentrum is acknowledged for the generous allocation of computer time. D.S. thanks the Auswärtiges Amt for a travel support, and C.R. is indebted to the University of Utah for a research grant.

References and Notes

(1) *Transition Metal Sulfur Chemistry*; Stiefel, E. I.; Matsumoto, K., Eds.; ACS Symposium Series 653; American Chemical Society: Washington, DC.

(2) (a) Yoon, J.-B.; Kim, S.-J. *Mech. Work. Steel Process. Conf. Proc.* **1997**, *34*, 425. (b) Hua, M.; Garcia, C. I.; DeArdo, A. J. *Metall. Mater. Trans. A* **1997**, *28A*, 1769. (c) Morita, M.; Hosoya, Y. *Mech. Work. Steel Process. Conf. Proc.* **1998**, *35*, 149.

(3) Jonsson, J.; Launila, O.; Lindgren, B. *Mon. Not. R. Astron. Soc., Short Commun.* **1992**, *258*, 49.

(4) An average of $D_0(Sc-S) = 4.93 \pm 0.13$ eV is derived from the values given in: (a) Coppens, P.; Smoes, S.; Drowart, J. *Trans. Faraday Soc.* **1967**, *63*, 2140. (b) Steiger, R. A.; Cater, E. D. *High Temp. Sci.* **1975**, *7*, 288.

(5) A value of $D_0(Ti-S) = 4.75 \pm 0.13$ eV has been derived by: (a) Smoes, S.; Coppens, P.; Bergman, C.; Drowart, J. *Trans. Faraday Soc.* **1969**, *65*, 682. (b) Pelino, M.; Viswanadham, P.; Edwards, J. G. *J. Phys. Chem.* **1979**, *83*, 2964.

(6) For descriptions of the methods, see: (a) Simard, B.; Mitchell, S. A.; Humphries, M. R.; Hackett, P. A. *J. Mol. Spectrosc.* **1988**, *129*, 186. (b) Weitzel, K.-M. *Ber. Bunsen-Ges. Phys. Chem.* **1998**, *102*, 989.

(7) For reviews on cationic transition-metal oxides, see: Schröder, D.; Schwarz, H. *Angew. Chem.* **1995**, *107*, 2126; *Angew. Chem., Int. Ed. Engl.* **1995**, *34*, 1973. (b) Schröder, D.; Shaik, S.; Schwarz, H. In *Metal-Oxo and Metal-Peroxo Species in Catalytic Oxidations*; Meunier, B., Ed.; Structure and Bonding, Vol. 97; Springer-Verlag, Berlin, 2000, in press.

(8) Shaik, S.; Danovich, D.; Fiedler, A.; Schröder, D.; Schwarz, H. *Helv. Chim. Acta* **1995**, *78*, 1393.

(9) Kretzschmar, I. Dissertation, TU Berlin D83, Shaker Verlag, Aachen, 1999.

(10) For related studies of VS^+, see: (a) Kretzschmar, I.; Schröder, D.; Schwarz, H.; Rue, C.; Armentrout, P. B. *J. Phys. Chem. A* **1998**, *102*, 10060. (b) Rue, C.; Armentrout, P. B., Kretzschmar, I.; Schröder, D.; Harvey, J. N.; Schwarz, H. *J. Phys. Chem.* **1999**, *100*, 7858.

(11) For other transition-metal sulfide cations, see: (a) McMahon, T. J.; Jackson, T. C.; Freiser, B. S. *J. Am. Chem. Soc.* **1989**, *111*, 421. (b) Harvey, J. N.; Heinemann, C.; Fiedler, A.; Schröder, D.; Schwarz, H. *Chem. Eur. J.* **1996**, *2*, 1230. (c) Kretzschmar, I.; Fiedler, A.; Harvey, J. N.; Schröder, D.; Schwarz, H. *J. Phys. Chem. A* **1997**, *101*, 6252. (d)

Kretzschmar, I.; Schröder, D.; Schwarz, H. *Int. J. Mass Spectrom. Ion Processes* **1997**, *167/168*, 103. (e) Brönstrup, M.; Schröder, D.; Schwarz, H. *Organometallics* **1999**, *18*, 1939. (f) Schröder, D.; Kretzschmar, I.; Schwarz, H.; Rue, C.; Armentrout, P. B. *Inorg. Chem.* **1999**, *38*, 3474. (g) Bärsch, S.; Kretzschmar, I.; Schröder, D.; Schwarz, H.; Armentrout, P. B. *J. Phys. Chem. A* **1999**, *103*, 5925. (h) Kretzschmar, I.; Schröder, D.; Schwarz, H.; Armentrout, P. B. In *Advances in Metal and Semiconductor Clusters − Metal−Ligand Bonding and Metal-Ion Solvation*; Duncan, M. A., Ed.; JAI Press Inc.: Stamford, submitted for publication.

(12) Ervin, K. M.; Armentrout, P. B. *J. Chem. Phys.* **1985**, *83*, 166.

(13) Schultz, R. H.; Armentrout, P. B. *Int. J. Mass Spectrom. Ion Processes* **1991**, *107*, 29.

(14) (a) Aristov, N.; Armentrout, P. B. *J. Am. Chem. Soc.* **1984**, *106*, 4065. (b) Aristov, N.; Armentrout, P. B. *J. Am. Chem. Soc.* **1986**, *108*, 1806. (c) Aristov, N.; Armentrout, P. *J. Phys. Chem.* **1987**, *91*, 6178. (d) Clemmer, D. E.; Sunderlin, L. S.; Armentrout, P. B. *J. Phys. Chem.* **1990**, *94*, 208.

(15) (a) Kemper, P. R.; Bowers, M. T. *J. Phys. Chem.* **1991**, *95*, 5134. (b) Haynes, C. L.; Armentrout, P. B. *Organometallics* **1994**, *13*, 3480.

(16) (a) Sunderlin, L. S.; Armentrout, P. B. *J. Phys. Chem.* **1988**, *92*, 1209. (b) Chen, Y.-M. Clemmer, D. E.; Armentrout, P. B. *J. Phys. Chem.* **1994**, *98*, 11490.

(17) (a) Schultz, R. H.; Crellin, K. C.; Armentrout, P. B. *J. Am. Chem. Soc.* **1991**, *113*, 8590. (b) Armentrout, P. B. In *Advances in Gas-Phase Ion Chemistry*; Adams, N. G., Babock, L. M., Eds.; JAI Press: Greenwich, 1992; Vol. 1, pp 83−119.

(18) The $m/z = 44$ in the Ar_2^+/CO couple and the $m/z = 64$ in the Ar_2^+/COS couple are believed to result from secondary reactions of the charge-transfer products CO^+ and COS^+, respectively.

(19) (a) Eller, K.; Schwarz, H. *Int. J. Mass Spectrom. Ion Processes* **1989**, *93*, 243. (b) Eller, K.; Zummack, W.; Schwarz, H. *J. Am. Chem. Soc.* **1990**, *112*, 621.

(20) FERETS = front-end resolution enhancement with tailored sweeps. See: Forbes, R. A.; Laukien, F. H.; Wronka, J. *Int. J. Mass Spectrom. Ion Processes* **1988**, *83*, 23.

(21) (a) Su, T.; Chesnavich, W. J. *J. Chem. Phys.* **1982**, *76*, 5183. (b) Su, T. *J. Chem. Phys.* **1988**, *88*, 4102. (c) Su, T. *J. Chem. Phys.* **1988**, *89*, 5355.

(22) The ADF package is available from: te Velde, G.; Baerends, E. J., Department of Theoretical Chemistry, Vrije Universiteit, Amsterdam, The Netherlands.

(23) Snijders, J. G.; Baerends, E. J. *Mol. Phys.* **1977**, *33*, 1651.

(24) Vosko, S. H.; Wilk, L.; Nusair, M. *Can. J. Phys.* **1980**, *58*, 1200.

(25) Becke, A. D. *Phys. Rev. A* **1988**, *38*, 3098.

(26) Perdew, J. P. *Phys. Rev. B* **1986**, *33*, 8822.

(27) Levy, M.; Perdew, J. P. *Int. J. Quantum Chem.* **1994**, *49*, 539.

(28) (a) Baranov, V.; Javahery, G.; Hopkinson; A. C.; Bohme, D. K. *J. Am. Chem. Soc.* **1995**, *117*, 12801. (b) Bouchoux, G.; Salpin, J. Y.; Leblanc, D. *Int. J. Mass Spectrom. Ion Processes* **1996**, *153*, 37.

(29) (a) Schröder, D.; Hrušák, J.; Hertwig, R.; Koch, W.; Schwerdtfeger, P.; Schwarz, H. *Organometallics* **1995**, *14*, 312. (b) Dieterle, M.; Harvey, J. N.; Schröder, D.; Schwarz, H.; Heinemann, C.; Schwarz, J. *Chem. Phys. Lett.* **1997**, *277*, 399.

(30) Gioumousis, G.; Stevenson, D. P. *J. Chem. Phys.* **1958**, *29*, 292.

(31) Miller, K. J. *J. Am. Chem. Soc.* **1990**, *112*, 8553.

(32) Su, T.; Bowers, M. T. In *Gas-Phase Ion Chemistry*; Bowers, M. T., Ed.; Academic: New York, 1979; Vol. 1, pp 84−118.

(33) Barnes, L. A.; Rosi, M. Bauschlicher, C. W., Jr. *J. Chem. Phys.* **1990**, *93*, 609. The D_e values calculated in this reference were converted to D_0 using ZPVE = 0.05 eV computed with B3LYP/6-311+G*. This level of theory predicts $D_0(Sc^+-CO) = 1.01$ eV.

(34) Meyer, F.; Armentrout, P. B. *Mol. Phys.* **1996**, *88*, 187.

(35) Clemmer, D. E.; Dalleska, N. F.; Armentrout, P. B. *Chem. Phys. Lett.* **1992**, *190*, 259.

(36) Harvey, J. N.; Diefenbach, M.; Schröder, D.; Schwarz, H. *Int. J. Mass Spectrom. Ion Processes* **1999**, *182/183*, 85.

(37) For investigations of systematic effects on the threshold analysis for low-energy CID processes, see: Hales, D. A.; Lian, L.; Armentrout, P. B. *Int. J. Mass Spectrom. Ion Processes* **1990**, *102*, 269.

(38) Sugar, J.; Corliss, C. *J. Phys. Chem. Ref. Data* **1985**, *14* (Suppl. 2).

(39) Heinemann, C.; Schwarz, J.; Schröder, D.; Schwarz, H. *Helv. Chim. Acta* **1996**, *79*, 1110.

(40) Comisarow, M. B.; Grassi, V.; Parisod, G. *Chem. Phys. Lett.* **1978**, *57*, 413.

(41) Moore, C. E. *Atomic Energy Levels*; National Standard Reference Data Series, NSRDS−NBS 35; National Bureau of Standards: Washington, DC, 1971.

(42) (a) Tilson, J. L.; Harrison, J. F. *J. Phys. Chem.* **1992**, *96*, 1667. For calculations of neutral ScS and TiS, see: (b) Bauschlicher, C. W., Jr.; Maitre, P. *Theor. Chim. Acta* **1995**, *90*, 189. (c) Bauschlicher, C. W., Jr.; Langhoff, S. R. *J. Chem. Phys.* **1986**, *85*, 5936.

(43) Sodupe, M.; Branchadell, V.; Rosi, M.; Bauschlicher, C. W., Jr. *J. Phys. Chem. A* **1997**, *101*, 7854.

(44) Werner, H. *Angew. Chem.* **1990**, *102*, 1121; *Angew. Chem., Int. Ed. Engl.* **1990**, *29*, 1077.

(45) (a) Saillard, Y.; Grandjean, D.; Caillet, P.; Le Beuze, A. *J. Organomet. Chem.* **1975**, *94*, 409. (b) Andrews, M. A. *Inorg. Chem.* **1977**, *16*, 497.

(46) Allred, A. L.; Rochow, E. G. *J. Inorg. Nucl. Chem.* **1958**, *5*, 264.

(47) Fisher, E. R.; Elkind, J. L.; Clemmer, D. E.; Georgiadis, R.; Loh, S. K.; Aristov, N.; Sunderlin, L. S., Armentrout, P. B. *J. Chem. Phys.* **1990**, *93*, 2676.

(48) Armentrout, P. B.; Clemmer, D. E. In *Energetics of Organometallic Species*; Simoes, J. A. M., Ed.; Kluwer: Netherlands, 1992; pp 321−356.

(49) Lias, S. G.; Bartmess, J. E.; Liebman, J. F.; Holmes, J. L.; Levin, R. D.; Mallard, W. G. *J. Phys. Chem. Ref. Data* **1988**, *17* (Suppl 1).